Review

3D Printed Multiphasic Scaffolds for Osteochondral Repair: Challenges and Opportunities

Stephanie E. Doyle [1,2,*], Finn Snow [1], Serena Duchi [2,3,4], Cathal D. O'Connell [1,2], Carmine Onofrillo [2,3,4], Claudia Di Bella [2,3,5] and Elena Pirogova [1,*]

[1] Electrical and Biomedical Engineering, School of Engineering, RMIT University, Melbourne, VIC 3000, Australia; s3718367@student.rmit.edu.au (F.S.); cathal.o'connell2@rmit.edu.au (C.D.O.)

[2] ACMD, St Vincent's Hospital Melbourne, Fitzroy, VIC 3065, Australia; serena.duchi@unimelb.edu.au (S.D.); carmine.onofrillo@unimelb.edu.au (C.O.); claudia.dibella@unimelb.edu.au (C.D.B.)

[3] Department of Surgery, The University of Melbourne, St Vincent's Hospital Melbourne, Fitzroy, VIC 3065, Australia

[4] ARC Centre of Excellence for Electromaterials Science, Intelligent Polymer Research Institute, University of Wollongong, Wollongong, NSW 2522, Australia

[5] Department of Orthopaedics, St Vincent's Hospital Melbourne, Fitzroy, VIC 3065, Australia

[*] Correspondence: sdoyle.email@gmail.com (S.E.D.); elena.pirogova@rmit.edu.au (E.P.)

Abstract: Osteochondral (OC) defects are debilitating joint injuries characterized by the loss of full thickness articular cartilage along with the underlying calcified cartilage through to the subchondral bone. While current surgical treatments can provide some relief from pain, none can fully repair all the components of the OC unit and restore its native function. Engineering OC tissue is challenging due to the presence of the three distinct tissue regions. Recent advances in additive manufacturing provide unprecedented control over the internal microstructure of bioscaffolds, the patterning of growth factors and the encapsulation of potentially regenerative cells. These developments are ushering in a new paradigm of 'multiphasic' scaffold designs in which the optimal micro-environment for each tissue region is individually crafted. Although the adoption of these techniques provides new opportunities in OC research, it also introduces challenges, such as creating tissue interfaces, integrating multiple fabrication techniques and co-culturing different cells within the same construct. This review captures the considerations and capabilities in developing 3D printed OC scaffolds, including materials, fabrication techniques, mechanical function, biological components and design.

Keywords: osteochondral; articular cartilage; calcified cartilage; subchondral bone; multiphasic; biofabrication; 3D printing

1. Introduction

The structure of the knee allows for mobility and load-bearing movements [1]. Within the joint, the bone surfaces are covered with smooth, continuous articular (hyaline) cartilage which assists in movement and distribution of load [2]. Articular cartilage lacks vascularization and has a low cell density which contribute to its very poor ability to self-repair, implying that damage to the cartilage (chondral defects) will remain impaired and unfilled over time [3–7]. In contrast, injuries that include the underlying subchondral bone may be filled with fibrocartilage if the vascularization system in the bone is damaged causing the release of cells and factors which trigger a repair response [5,7–9]. Chondral defects can occur due to trauma or surgery or can arise idiopathically through general wear and tear during aging. Such defects are graded according to severity, each with their own treatment or pain-management strategies. OC defects are among the most severe and debilitating cases and are characterized by the complete loss of cartilage (articular and calcified) down to the underlying subchondral bone. OC defects have been detected in up to 20.8% of knee arthroscopies [10–15]. Without the ability to fully self-repair, empty

OC defects can alter how forces are distributed over the joint and the areas where stress is concentrated [16]. Peak stress concentration can in turn accelerate the breakdown of the tissue surrounding the defect, leading to osteoarthritis [16].

Current surgical treatments for a full OC defect are limited and include microfracture or transplantation of OC tissue (allograft or autograft) [17,18]. While these treatments can provide some initial relief from pain, they have shown significant limitations, thus motivating research into regenerative approaches targeting full restoration of the damaged tissues as a long-term solution [19,20].

Tissue engineering strategies aim to restore tissue function using methods which combine cells, tissue-inducing agents (such as growth factors) and a scaffold (typically a biomaterial structure designed to guide regeneration) [21]. Cartilage and bone tissue engineering has been pursued since the 1990s, with most developed approaches based on highly simplistic, monolithic representations of each tissue type. In recent years, additive fabrication technologies have emerged, providing new tools for engineering living tissues, including bone and cartilage [22,23]. This adoption of additive fabrication techniques for the regeneration of living tissues has created the new subfield termed 'biofabrication' [24]. Biofabrication strategies offer enhanced control over the microstructural environment of engineered tissue by modulating the material(s), the structural design and the distribution of biological components. Such capabilities are especially relevant for recapitulating tissue interfaces, including the OC unit, since each respective tissue can be tailored to achieve the specific architectural framework and bioactivity [25].

With this rapid evolution of technology, recent reviews of OC regeneration have surveyed various specific aspects, including material focused; hydrogel-based 3D printed scaffolds, bioactive composite scaffolds, and fabrication method focused; scaffolds made via solid free-form techniques, printability requirements for OC bioinks [22,26–28]. In contrast, this review focuses holistically on recent advances in multiphasic additive manufactured OC scaffolds, including their main constitutive elements, i.e., materials, fabrication method, mechanical function, biological components and design. The articles reviewed here are limited to those that target the repair of the entire OC unit and exclude those which only address one of the three tissues individually (e.g., chondral defects only).

First, we describe the composition of native OC tissue and introduce current treatment methods. We then describe recent advances in engineering the OC tissue, with a particular focus on additive fabrication techniques. We next describe the methods for evaluating engineered OC tissue in vitro and in vivo, and finally conclude with a broader assessment of the field and future outlook.

2. Osteochondral Tissue: Anatomy, Pathology and Treatments

2.1. Structure of Osteochondral Tissue

The native OC tissue consists of three different regions: the articular cartilage, the subchondral bone and the calcified cartilage-the interface or transition region in between. The three distinct regions have differing material compositions, fiber orientations and cell populations (Figure 1), and mechanical properties (Table 1). The articular cartilage can be further divided into the superficial, middle and deep zones, each with its own idiosyncratic microstructure determined by the extracellular matrix (ECM) structure and composition; chondrocyte number, shape and orientation; collagen type, and proteoglycan orientation (Figure 1) [29,30].
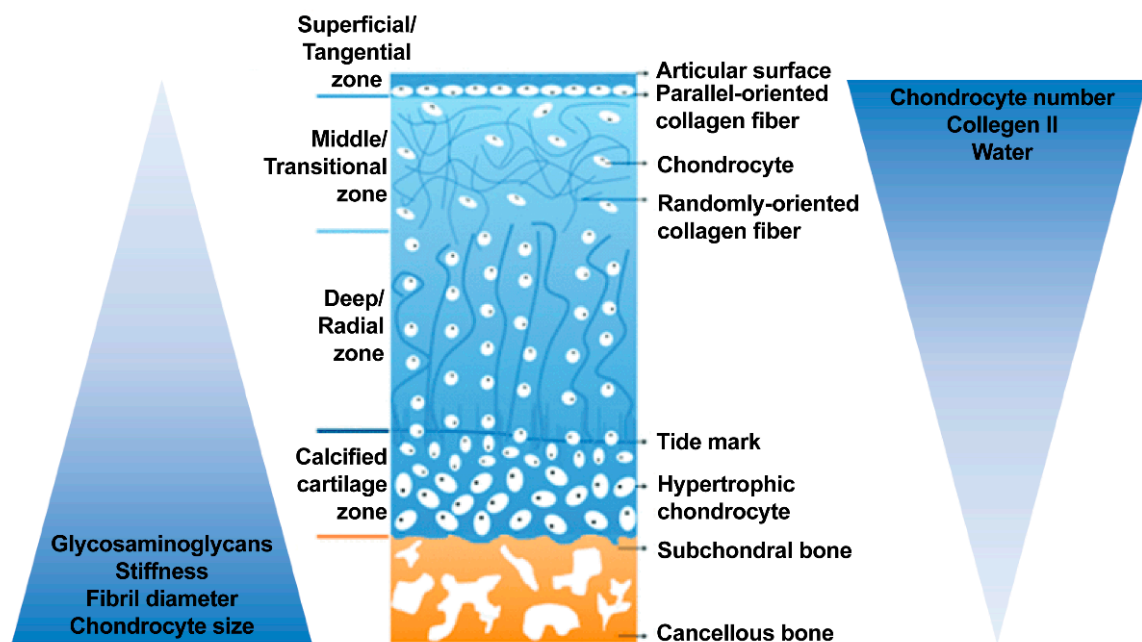
Figure 1. Gradient schematic of the OC tissue [31,32]. While the OC tissue is made up of articular cartilage, calcified cartilage and subchondral bone, each of these tissues are not homogenous. Especially in the articular cartilage, each zone within varies in cell size, number and orientation as well as collagen fiber size and orientation. Overall trends of the full OC unit are summarized in the ascending and descending triangles.

Table 1. Compressive-based mechanical properties of the human OC tissue.

OC Region	Mechanical Test	Elastic/Young's Modulus	Ref
Articular Cartilage	Indentation	1.03 ± 0.48 Mpa	[33]
	Unconfined compression	0.854 ± 0.348 MPa	[34]
		0.64 ± 0.30 MPa	[35]
Calcified Cartilage	Indentation	6.44 ± 1.02 MPa	[36]
Subchondral Bone	Indentation	≈6–13 GPa	[37]
	Unconfined compression	297–475 MPa	[38]
	Unconfined compression via finite element modelling	3–20 GPa	[39]
		296 ± 107–497 ± 52 MPa	[40]

2.1.1. Articular Cartilage

The average thickness of human articular cartilage varies depending on the site within the joint and the age of the patient. Hunziker et al. found the average human articular cartilage to be 2.41 ± 0.53 mm, but patients with joint diseases can display a decrease in thickness down to 1.48 ± 0.075 mm [36,41]. Despite being broken down into zones, the articular cartilage is a continuous region described as a 'porous composite organic solid matrix swollen by water' [42]. The mesoporous tissue has an average pore size of 6 nm which allows free water to move [42].

The outermost surface of the joint, the superficial or tangential zone, has the role of distributing loads evenly across its surface [43]. The chondrocytes residing in this zone are relatively small, flat and collagen fibrils are arranged parallel to the articular surface (Figure 1) [44,45]. Furthermore, the superficial zone has the highest deformation capability (out of three zones) and therefore is able to exchange fluids with the neighboring environment to better respond to compressive forces applied to the joint [45]. The middle or transitional zone provides some resistance to compressive force; the collagen fibrils contained in this area are not clearly orientated; proteoglycan content is the highest and chondrocytes are large and spherical in a loose columnar arrangement (Figure 1) [2,45–48]. The deep or radial zone provides the tissue with its greatest ability to withstand compressive forces

due to collagen fibrils which run perpendicular to the cartilage surface [2,45,49,50]. The chondrocytes here are also arranged in perpendicular stacks (Figure 1) [43]. Water content is the lowest, and permeability is also lower compared with the superficial zones [45,51].

2.1.2. Calcified Zone and Tidemark: The Transition/Interface

The calcified zone is made up of ≈22% unmineralized tissue which contains porous structures and then ≈88% mineralized tissue and, along with the subchondral bone, assists with shock absorption in the joint [52–54]. A few chondrocytes present in the calcified zone have limited metabolic activity and synthesize collagen type X, which can calcify the ECM [55]. The collagen fibrils run from the deep zone through the tidemark and calcified zone before anchoring to the subchondral bone with an orientation perpendicular to the tidemark [29,30,53]. The tidemark is a distinguishable line within the calcified zone which separates the calcified from the uncalcified articular cartilage with few to no cells [30,56,57]. The transitional property of calcified cartilage can be seen in its composition, at 65.1% hydroxyapatite (HA) dry weight for the calcified layer compared to 0% and 85.8%, respectively, for articular cartilage and subchondral bone [53,58].

2.1.3. Subchondral Bone

The subchondral bone provides support by maintaining the joint shape, resisting stress and providing shock absorption as well as delivering nutrients through its vascular network [59,60]. The vascular structure in bone provides some limited regenerative capabilities as immune response cells and a cocktail of cells (osteoblasts, osteoclasts, osteocytes, chondrocytes, endothelial and mesenchymal stem/stromal cells (MSCs)) are present in this tissue and can be delivered directly to the area of impact [30,53,61]. Despite many cell types present in the subchondral bone, osteocytes are the most prominent (90–95% of total cells in the region) and are responsible for controlling signals to osteoblasts (bone formation) and osteoclasts (bone resorption) [53,62]. As a form of spongy bone, subchondral bone exhibits a low bone volume fraction of 6–36% resulting in a high porosity [63]. With some varying definitions of the term 'subchondral bone', in this review, we refer to subchondral as the region under the calcified cartilage [64].

2.2. Existing Surgical Treatments for Osteochondral Defects

There are currently limited surgical options to repair an isolated OC defect [65,66]. In contrast, chondral-only defects have more surgical options available, including the tissue engineering techniques of autologous chondrocyte implantation and matrix-induced autologous chondrocyte implantation. However, these techniques are only focused on the repair/regeneration of the cartilage, while defects greater than 6–8 mm in depth (OC defects) require the addition of a bone graft [18]. Instead, relatively small OC defects, <2 cm^2, can be treated using microfracture surgery where holes are created in the subchondral bone to access the bone marrow and release stem cells and growth factors (Figure 2A) [17,67–70]. While this method can produce new cartilage, histological analysis shows this to be mostly composed of fibrocartilage [70] which lacks the lubricative and load distribution properties typical of the native articular hyaline cartilage [54].

The conventional approach for the repair of OC defects is whole tissue transplantation (Figure 2B) [18], either as an autograft or allograft.

Osteochondral autograft transfer (OAT), also known as mosaicplasty, involves the transfer of OC cylindrical plugs from a non-weight bearing region of the patient's joint to the defect (Figure 2C) [71–75]. While OAT can relieve pain in many patients, [76] the results are considerably less satisfactory when the defect is outside of a specified size range (typically 1–4 cm^2 is recommended) or for patients over 35 [77–81]. One issue is how gaps between the plug(s) and the host cartilage can allow inflamed synovial fluid to penetrate and limit the healing and integration of the graft [82,83].

Osteochondral allograft transplants (OCA) involve transplanting an OC graft from a donor (bone bank) and is recommended for larger defects, greater than 2–4 cm^2

(Figure 2D) [79,80,84]. As with OAT, the plugs of native tissue consist of all three OC tissues: articular cartilage, calcified cartilage and subchondral bone, with an overall height of the plug to match that of the defect. While OAT will often require multiple smaller plugs to fill a defect, OCA generally uses a single, larger plug, cut to size to match the defect shape [79]. However, issues with variability in tissue preparation and storage, infection, allograft/host mismatch, implant failure and arthritic degenerative changes, remain a significant limitation of this technique [85,86]. The risk of implant failure also increases for patients over 35 years old or who are female [86,87].

Of these existing treatments, only microfracture can facilitate new tissue growth, however, it does not produce the required hyaline-type cartilage. The average OC defect size reported in the literature is 4.1 cm^2, which is above the recommended size for an OAT procedure [77]. The lack of an existing treatment with long term-effectiveness, particularly for larger OC defects, drives research towards a tissue engineered solution.
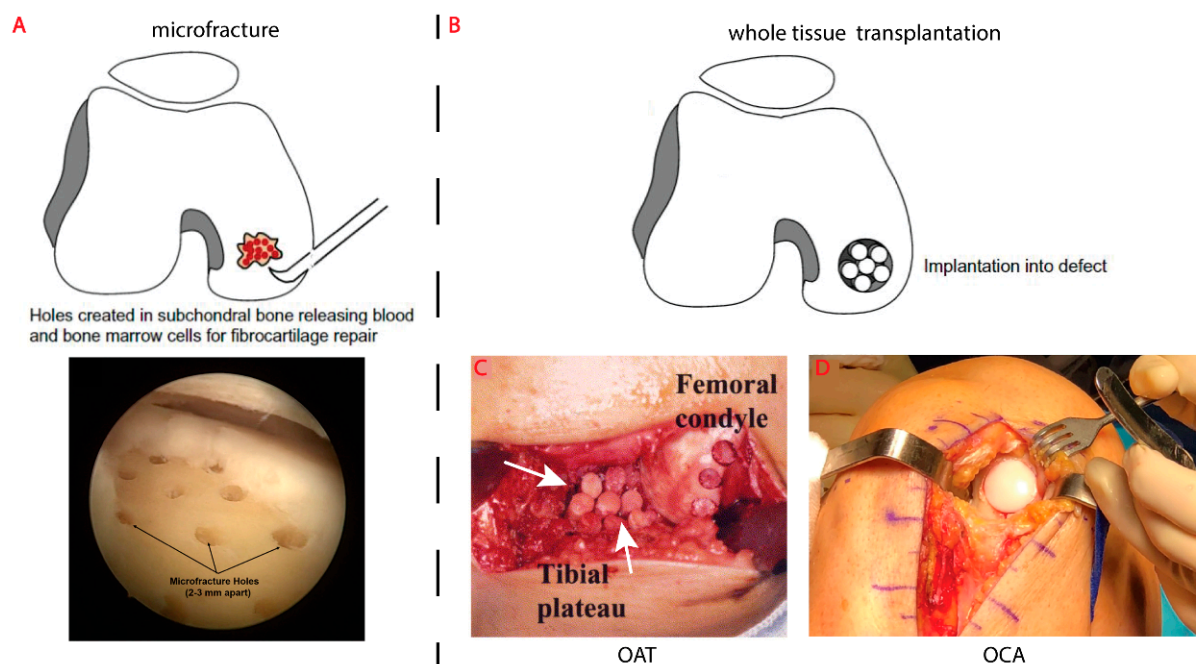

Figure 2. Current surgical techniques for the repair of an OC defect. (**A**). Microfracture [88] facilitate the repair of new tissue but primarily consists of fibrocartilage which fails to mimic the function of the native tissue [89]. (**B**). Whole tissue transplantation [88] of the mature OC unit can be from a patient (OAT) (**C**) [77] or from a donor (OCA) (**D**) [79]. The multiple plugs commonly used in OAT leaves gaps between plugs as well as between the plug and the host tissue (white arrows).

3. Engineering New Osteochondral Tissue

The aim of an OC scaffold is to trigger the growth of new tissue in all its aspects, therefore mimicking the characteristics of the articular cartilage, calcified cartilage and subchondral bone. The scaffold must have the following functions: create a biocompatible environment, possess the mechanical function close to the native tissue, provide differential biological stimuli to address the lineage specific differentiation of implanted cells and production of the desired ECM, and possess the ability to integrate with the host tissue. Considering these requirements, we identified the following essential elements for the generation of the OC scaffold: material/s, fabrication method, mechanical function, biological component and scaffold design (Figure 3).
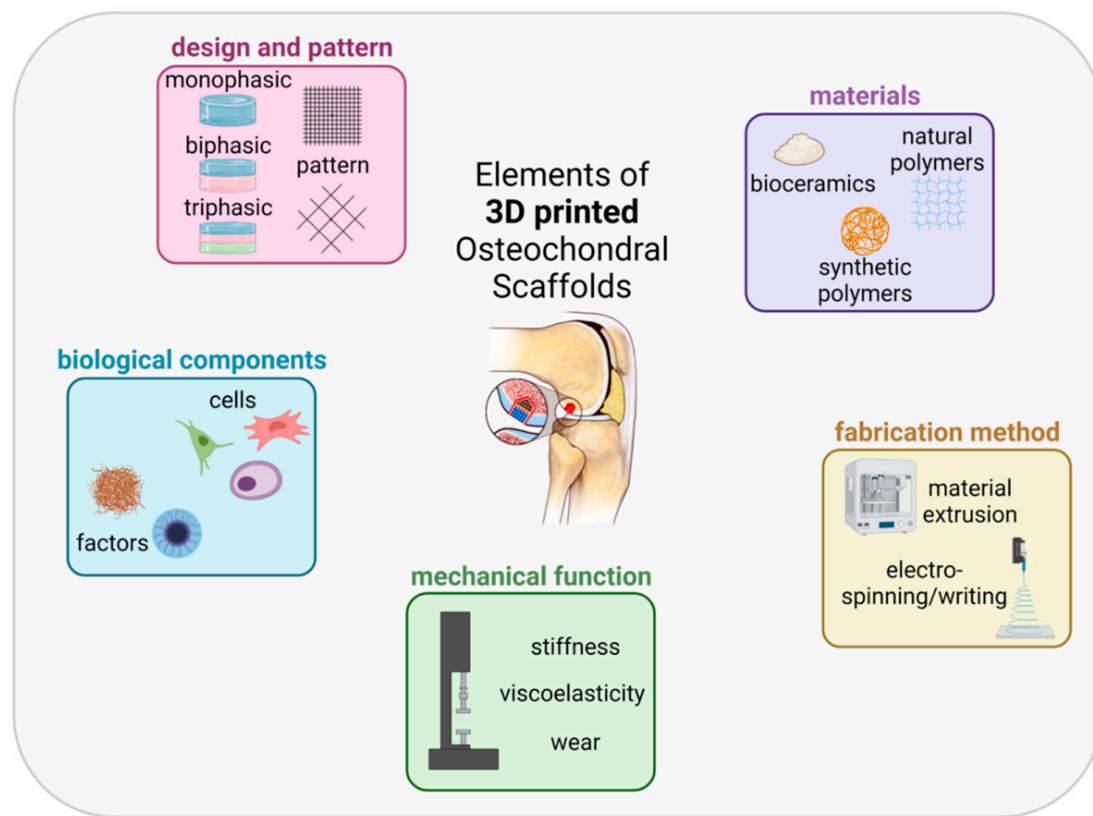
Figure 3. Elements of 3D printed OC scaffolds. We have identified five main domains of a 3D printed OC scaffold: materials (e.g., natural and synthetic polymers, bioceramics and hydrogels), fabrication method (e.g., material extrusion (ME), electro-spinning (ES), electrowriting and stereolithography (SLA), mechanical function, biological components (e.g., cells–chondrocytes, osteoblasts, stem cells and growth factors) the overall design (e.g., mono or multiphasic) and pattern of each 3D printed layer. Figure created with BioRender.com (10 October 2021).

3.1. Elements of an OC Scaffold: Materials

Numerous scaffold criteria, such as biodegradability, processability, osteoinductivity, facilitating chondrogenesis, biocompatibilty and mechanical suitability can be adequately met via the correct selection of material(s) [90]. The materials that satisfy these criteria and are commonly utilized in OC scaffolds include natural and synthetic polymers and bioceramics, either alone or in combination [91].

3.1.1. Natural Polymers

In OC engineering, natural polymers are commonly used in hydrogel form where their polymer networks are capable of holding a large amount of water thereby creating a fully hydrated 3D environment, comparable to that of the natural ECM [92,93]. This environment can support cell adhesion, proliferation and differentiation of various cells [94]. On the other hand, natural polymers typically possess weak mechanical properties, which can lead to deformation in weight bearing areas [95].

The base polymers processed from natural sources and widely used in OC scaffolds are gelatin, alginates, collagens and hyaluronic acid [96–110]. Of note, these natural materials are commonly modified, especially to allow for crosslinking (e.g., gelatin to gelatin methacryloyl (GelMA), hyaluronic acid to hyaluronic acid methacrylate) and as such become categorized as semi-synthetic materials [111,112]. Hyaluronic acid is typically used in the cartilage phase as it is a main component of the native cartilage ECM [102]. The weak mechanical properties are regularly emphasized as well as strategies to overcome this limitation include combining with another class of material or a reinforcement structure [96,98,105,108,110,113].

3.1.2. Synthetic Polymers

Key advantages of synthetic polymers are enhanced mechanical properties (strength and stiffness) as well as their controllable biodegradability and processability [114]. However, synthetic polymers offer no specific biological influence over cells [115]. Polycaprolactone (PCL) is overwhelmingly used across all three phases of the OC scaffold, both on its own and when combined with other materials, due to its tunable biodegradability and approval by regulatory bodies, such as the Food and Goods Administration [98,99,101,103–106,110,116–118]. Polylactic acid (PLA) and poly(L-lactic-co-glycolic acid) (PLGA) are also used in all phases of the OC scaffold [104,119–122]. Critchley et al., compared the mechanical properties of PCL, PLA and PLGA (65:35 and 85:15 lactic acid to glycolic acid) in cartilage phase scaffolds [110]. After 21 days under physiological conditions, they found the PLGA 65:35, PLGA 85:15 and PLA had approximately a 956, 4.8 and 2.7 fold decrease in mechanical properties while the PCL did not change [110]. This finding highlights concerns of the suitability of PLGA in a load bearing joint due to its fast degradation rate and therefore rapid decrease in stiffness.

The hydrogel of synthetic origin, most commonly used in OC engineering, is polyethylene glycol (PEG) based, and these hydrogels are primarily used in the cartilage region of the scaffold [101,123–125]. PEG is an inert hydrogel providing a 'blank canvas' for modifying the degradation rate, mechanical properties and introducing biological drivers [125–127].

3.1.3. Bioceramics

The category of bioceramics includes bioactive ceramics, bioactive glasses and bioresorbable ceramics which are primarily used in the bone phase and, to a lesser extent, the calcified cartilage phase of an OC scaffold [128]. Calcium phosphate cements and pastes, HA and tricalcium phosphate (TCP) are the most commonly used bioceramics [97–99,102–105,108,109,113,123,129–131]. These materials naturally exist as a brittle powder, thereby limiting their ability to form free-standing porous structures on their own [132]. Each material, formulation, source, and synthesis method within the category have varying levels of osteointegration, biomineralization, osteoinduction and osteoconduction capabilities [132–134]. In the study comparing PCL composites with various bioceramics, decellularized bone matrix, a natural product, was found to be more osteoinductive then its synthetic counterparts HA and TCP, but these natural products are not commonly used in OC engineering [135].

Any combination of these material classes can be used with one another in order to minimize the undesirable properties and maximize the favorable ones. The use of multiple materials, especially in multiphasic scaffolds, allows the native OC environment to be more closely biomimetic.

3.2. Elements of an OC Scaffold: Fabrication Method

Selection of the fabrication method and material selection are interconnected and codependent steps within the OC scaffold design process. For example, when selecting a material, capabilities and compatibility of the suitable fabrication method should be taken into consideration (and vice versa). A single fabrication method can be used to create the entire OC scaffold or different methods can be used for creating the different phases. The most widely used additive manufacturing techniques for creating 3D printed OC scaffolds are ME, Melt Electro-Writing (MEW), ES, SLA and Digital Light Processing (DLP) [136]. Of note, this review captures only the commonly used 3D printing methods; however new 3D printing techniques are constantly emerging, including cyrogenic 3D printing [137], powder-based printing [138,139], indirect printing [140–142], phase separation [121] and custom-built printers [143].

In the native tissue, the articular cartilage is continuous, with an average pore size of only 6 nm, calcified cartilage has pores within the unmineralized areas which accounted for ≈22% of the tissue and subchondral bone has an overall porosity of 64–94% [42,52,63].

Using the native tissue as a template can guide the selection or suitability of each fabrication technique for each region of the OC scaffold.

3.2.1. Material Extrusion

ME involves moving material through a nozzle to deposit it onto a print bed first on the XY plane before stepping up in the Z plane and continuing in a layer-by-layer fashion. As such, in standard ME printing, all material deposited needs to be (at least partially) physically supported by either the previous layers, support material or support bath [144].

ME printing allows for a broad range of materials to be used, including thermopolymers, hydrogels and bioceramics, where each category, material or composite, requires fine tuning of printing parameters, such as temperature, extrusion pressure, print speed and crosslinking or gelation for hydrogels [145–148]. ME allows for creating relatively porous scaffolds that enable cell proliferation and tissue ingrowth [149,150]. Smaller pores (<0.1–0.3 mm) can assist with neocartilage formation, and larger pores (>0.3 mm) can facilitate cell and bone growth [15–153].

The capabilities of thermopolymer-based ME (Figure 4A,H,K) are in creating porous structures which is most relevant to the subchondral bone phase. In the subchondral bone phase of multiphasic OC scaffolds, pore size is widespread between 0.3–1.0 mm, while the porosities lie between approximately 70–80% [103,106,130,154]. These indicative capabilities of ME extrusion with thermopolymer-based materials (the porosity range of subchondral bone and the pore size) were suggested to facilitate bone growth.

Bioceramic-based ME (Figure 4I,M) is also primarily used for the subchondral phase of the OC scaffold [105,109,155–157]. Overall, achievable porosities are lower in bioceramic printed scaffolds (≈20–60%) then thermopolymer printed ones (≈70–80%), which highlights the difficulties in creating high-porosity scaffolds with bioceramics-based materials. Pore size is also reduced (0.1–0.4 mm), with many scaffolds failing to produce the >0.3 mm pore size to facilitate bone growth in the subchondral bone phase [105,155,156]. Therefore, while the technique is widely used to create the subchondral bone phase of the OC scaffold, the ramifications of low porosity and pore size on tissue growth are not often displayed.

Hydrogel-based scaffolds in OC engineering (Figure 4B,I,J,L) are more commonly produced by simple casting techniques, especially on top of a 3D printed phase for the cartilage phase, and less commonly 3D printed to provide a specific architecture. This is likely due to the desire to mimic the continuous nature of the native articular cartilage. In addition, when employing biomimicry, physical characterizations such as such as the macro, meso and micro-porosity of the hydrogel are more relevant than pore size and porosity because these measurements are not used to describe the native tissue [103,158,159]. Kilian et al., produced the intermediate result between casting and 3D printing approaches by printing their hydrogel cartilage phase in a strand-wise pattern, thereby achieving a continuous layer [109]. The internal pore size depends largely on the material and is ranged between 100–800 nm and 100–220 μm, for alginate-based and GelMA 3D printed cartilage phases, respectively [103,108]. While larger than the pore size of native cartilage, the large pores can facilitate the distribution of nutrients, oxygen, the removal of waste and formation of neocartilage [103,108,151]. Despite hydrogel ME printed structures being commonly used in the cartilage phase, Gao et al., produced a biphasic OC scaffold entirely from hydrogel-based ME printing [113]. The subchondral bone phase included β-TCP in the base hydrogel which increased the stiffness and osteoinductive properties of the printed hydrogel, while the cartilage phase included transforming growth factor (TGF)-β1 to enhance chondrogenic differentiation [113].

3.2.2. Melt Electro-Writing and Electrospinning

MEW and ES also involve passing filament through a nozzle in a layer-by-layer deposition. However, in these techniques, voltage is used to control and continuously draw the filament onto the collector bed [160]. While fiber sizes range from the micrometer to nanometer scale, in practice MEW routinely produces micrometer fibers, while ES regularly

produces nanometer fibers [161,162]. Furthermore, ES is a solvent-based technique that randomly deposits lines of material onto the collector bed; whereas MEW is a solvent-free approach that controls where and how the fibers are deposited, therefore providing control over the resulting pattern [162]. For MEW and ES, the material choice is driven by those that are processible following the electrohydrodynamic principles that guide both techniques [163,164]. PCL remains the most widely used material for MEW, while a broader range of materials, including PCL, gelation, chitosan, polyvinyl alcohol (PVA), HA and collagen are incorporated in ES [106,163,165,166]. Despite the increase in materials used in ES, the solvents used are typically toxic which can present a concern if toxic residues are left behind [167,168].

A challenge when applying MEW and ES to OC scaffolds is in creating tall 3D structures as a charge builds-up which limits the ability to have a stable jet of material in the Z direction [169,170]. This limitation, has been addressed to increase the height of produced structures by printing onto various collector beds and objects [164,169,171].

What does this mean for OC scaffolds? Given the limited height and micro/nano fibers produced, MEW and ES generally create softer scaffolds and thus have mainly been applied in creating the cartilage or the calcified cartilage phase (Figure 4C,D,N).

Highlighting the height limitations, Cui et al., applied ES to create a full, monophasic OC scaffold and while the 2–3 mm thickness was sufficient to fill a full OC defect in a rat model, this translates to the range of a chondral-only defect in humans [77,172]. Using these techniques in combination with other fabrication methods, printing onto non-flat collector beds or stacking scaffolds, Liu et al., and Hejazi et al., produced OC scaffolds at heights of ≈6 mm and 15 mm, respectively, which is suitable for the full repair of human OC defects [99,165].

3.2.3. Stereolithography and Digital Light Processing

SLA and DLP also create 3D objects by layer-by-layer material deposition. However, these techniques are not nozzle-based, and instead the liquid material sits in a resin bath where a build plate is lowered in and a light source traces the programmed pattern, crosslinking only the relevant design. The process continues the material deposition layer after layer until the object is completed.

The difference between SLA and DLP is the light source used. SLA utilizes a laser, while DLP uses light from a projector [173]. SLA/DLP can routinely print feature sizes of 50 μm, therefore placing the technique between MEW/ES and ME in terms of the resolution [174,175]. These techniques can be compatible with many of the same base materials previously outlined. However, extensive modification of the material is typically required which can greatly change the properties of said material [176–179]. Materials used in OC scaffolds include PEG based (commonly PEG-diacrylate), GelMA and TCP which are mixed with any combination of photoinitiators, photoabsorbers, solvents and/or dispersants [103,123,125,180,181]. In OC scaffold generation, SLA and DLP printing is not used as widely as ME, potentially due to the greater upfront and ongoing costs of these systems, limited biomaterials readily available or challenges in multi-material printing [180,182]. However, new research continues to emerge to overcome these issues, such as custom printers or new materials [182].

So far, SLA and DLP printed OC scaffolds (Figure 4E–G,O) have not been shown to offer advantages in scaffold porosity (≈50–65%) compared to the other techniques; however, Gong et al., used DLP to produce a radially orientated hydrogel cartilage phase which assisted with cell infiltration [103,125,181]. These techniques can also be used to create the entire OC scaffold as demonstrated by Zhu et al., who used DLP to create a monophasic OC scaffold from a PEG-based material combined with native bovine cartilage ECM [125].
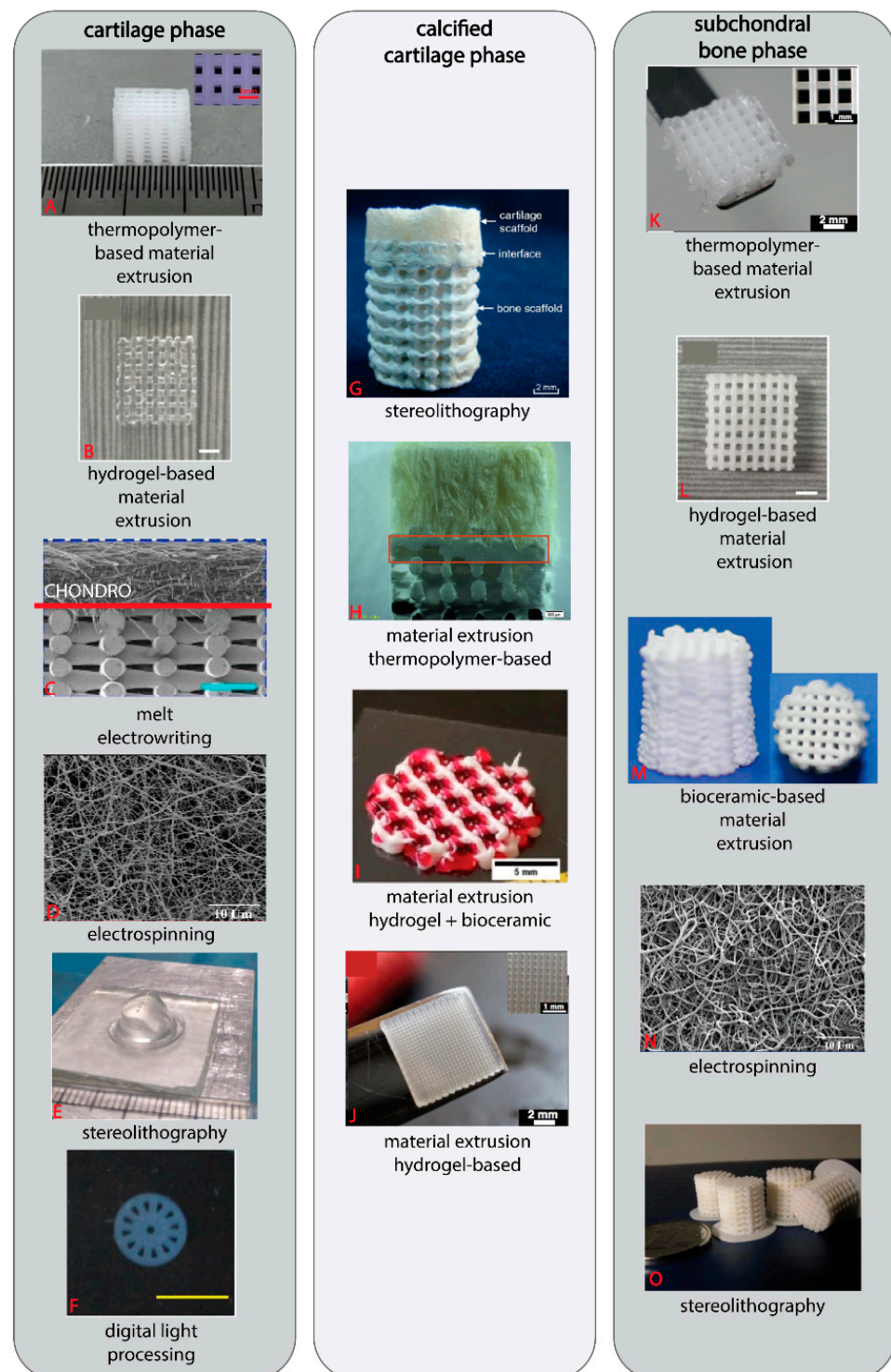
Figure 4. OC scaffold phases made via various 3D printing techniques. Some techniques, such as ME printing for thermopolymers and hydrogels, are commonly used across all phases of the OC scaffold, while other techniques, such as MEW, are commonly used only in one or two phases (cartilage and calcified cartilage). (**A**) Insert scale bar = 1 mm [183]. (**B**) Scale bar = 2 mm [113]. (**C**) Scale bar = 1 mm [184]. (**D**) Scale bar = 0.01 mm [165]. (**E**) [123]. (**F**) Scale bar = 5 mm [103]. (**G**) Scale bar = 2 mm [181]. (**H**) Scale bar = 0.5 mm [143]. (**I**) Scale bar = 5 mm [109]. (**J**) Scale bar = 2 mm, insert scale bar = 1 mm [104]. (**K**) Scale bar = 2 mm, insert scale bar = 1 mm [104]. (**L**) Scale bar = 2 mm [113]. (**M**) [156]. (**N**) Scale bar = 0.01 mm [165]. (**O**) [123].

3.3. Elements of an OC Scaffold: Mechanical Function

OC tissue primarily serves a mechanical, load-bearing function in the body. It is known that OC defects can change the distribution of forces across the joint, particularly for defects ≥10 mm in diameter [16]. Stress can concentrate near the rim of the defect, allowing the defect to grow in size if left untreated. The ultimate purpose of a biofabricated implant is to restore this load-bearing function and prevent further degradation. Thus, the mechanical function of an OC implant may be a critical factor in determining the success or failure of the intervention–especially in the immediate months after implantation, where the repair scaffold has not yet been able to produce mature tissue. In time, the new mature tissue may take over the mechanical function of the implanted scaffold in degradable scaffolds. However, the immediate stiffness mismatch or inadequate tuning of the degradation profile of the scaffold to that of the production of mature tissue, can cause the implant to fail due to the increased foreign body reaction and inflammatory response or large differences in the way the implant and tissue respond to applied forces [185–188]. This is in contrast to strategies, such as internal fixation devices, which are non-degradable and designed to retain their function immediately and over the life of the device/treatment (that may include prolonged load bearing and full range of motion of the joint) [189]. As such, the potential stiffness mismatch from the time of implantation is still an issue of consideration. The properties of the native tissue (Table 1 and colored bands Figure 5) are dependent on the mechanical test type, however the elastic modulus of human articular cartilage and subchondral bone (under unconfined compression) are approximately 0.64–0.854 MPa and 297–475 MPa, respectively, while calcified cartilage is ≈6.44 MPa under indentation [34–36,38]. As discussed, the negative implications of the stiffness mismatch between the implant and native tissue, as well as large variations in stiffness between each native OC regions are further justifying the need for a multiphasic OC scaffold, where, among other properties, the mechanical function can be designed to address the specific requirements of each constitutive region.

In addition to the multiphasic scaffold, the appropriate selection of material and fabrication method can minimize the ultimate stiffness mismatch as seen in Figure 5, where hydrogels are suited for softer structures, while thermopolymer and ceramic based ME are suited for stiffer structures.

For monophasic scaffolds, Wei et al., created a thermopolymer-based scaffold with a porosity of 75–79% and compressive modulus of 216–234 MPa. Hu et al., developed a natural polymer-based scaffold, with a porosity of 85–87% and compressive modulus of 4.16–7.59 MPa [190,191]. However, these homogenous scaffolds do not possess the ability to capture the different mechanical properties of each region of the native tissue.

Some research outputs provide a clear discussion on whether their OC scaffolds reach their desired mechanical function. For example, Chen et al., created a monophasic, ceramic-based scaffold (37–61% porosity) with a compressive strength of 15–40 MPa which, as reported, was sufficient and comparable to cancellous bone (2–12 MPa) [156]. Wang et al., noted that a high compressive strength would be desirable to induce differentiation in MSCs and their biphasic, thermopolymer-based OC scaffold showed an elastic modulus of 1.05, 14.1 and ≈6 MPa for the cartilage, bone and combined scaffold, respectively [192]. The thermopolymer-based scaffold (21–57% porosity) by Bittner et al., aimed to match the mechanical function of the 'native tissue'. The reported compressive modulus of 102 ± 7 MPa of their scaffold is within the range of human trabecular bone [193]. Each research group has stated to meet their mechanical property targets. However, the absolute values, if provided, for each target tissue, were greatly varied due to different reference sources as well as using values from the native human vs. animal tissue which resulted in large variability in outputs between groups (Figure 5). While it would be logical for the mechanical function and values of native human OC tissue to serve as the benchmark, this is often not the case.
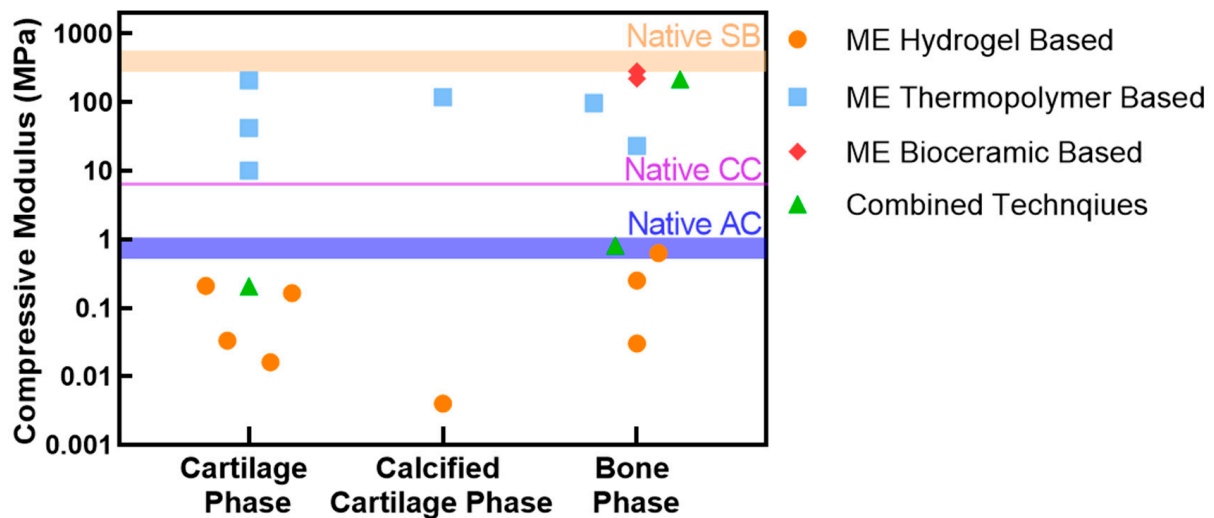
Figure 5. Compressive modulus of each phase of the OC scaffold. Data is limited for the calcified cartilage; however, the range of compressive modulus is similar regardless of the phase. Mechanical data for individual phases of the OC scaffold was also limited in techniques beyond ME. The bands represent the native tissue as from Table 1. Combined techniques refer to when multiple fabrication techniques are used to create the phase, e.g., ME thermopolymer scaffold filled with a hydrogel. Note: the band of the calcified cartilage (CC) is from indention and not compression of the whole tissue as for the articular cartilage (AC) and subchondral bone (SB). [96,97,99,104,113,121,183,193].

3.4. Elements of an OC Scaffold: Biological Components

The biological aspects of an OC scaffold include the elements placed within the construct, such as cells and growth factors as well as the culture conditions.

3.4.1. Considerations of Cell Type

The use of cells within an OC scaffold can be a homogeneous or heterogenous approach, with one or multiple cell types used. Cells specifically used in the cartilage and subchondral bone region include chondrocytes, chondroprogenitor cells and osteoblasts, while the most common cell type used across the entire OC scaffold are MSCs of different species and sources [100,102,105,106,109,194–197]. While MSCs are multipotent, induced pluripotent stem cells are, as the name suggests, pluripotent and therefore offer the ability to repair all the different OC tissue regions. However, to date this cell type has been rarely used in conjunction with 3D printed scaffolds for OC repair, potentially due to challenges in achieving uniform cell differentiation or highly variable results in chondrogenesis as well as increased regulatory hurdles with induced pluripotent stem cells [198–201]. Alternatively, the challenge with chondrocytes includes their ability to dedifferentiate and thereby stop or minimally produce collagen II which is the main component in hyaline cartilage [202,203]. In the development of OC scaffolds, both osteoblasts and chondrocytes are derived from the mesoderm, suggesting the potential to populate a multiphasic OC scaffold with a homogenous population of MSCs, which are then directed along alternate differentiation pathways using the tailored microenvironment within each phase. This strategy was employed by Liu et al., where bone marrow derived MSCs (bmMSCs) were present in each phase of the OC scaffold [102]. The scaffolds were subcutaneously implanted in rats, and after two months chondrogenic and osteogenic differentiation were achieved in the respective phases due to the targeted materials and controlled release of stem cell differentiation inducers [102]. This strategy presents new opportunities along with the complexities further discussed below.

3.4.2. Culture Conditions and Growth Factors

Cells, grown in vitro, require specific conditions to grow and proliferate, let alone differentiate. This involves tuning conditions, such as oxygen content, media type (in-

cluding the base media, serums and additional factors) and concentration, and regular media replacement [204]. The addition of physical cues, such as mechanical, electrical and electromagnetic, can influence cell signaling pathways and affect chondrogenesis or osteogenesis. Balancing all these conditions becomes even more challenging when multiple cell types are involved.

Growth factors also aim to influence cell behavior such as growth, proliferation and differentiation [205,206]. Growth factors, relevant to supporting neocartilage formation, include insulin-like growth factor (IGF) 1, bone morphogenetic proteins (BMP) 2 and 6, BMP-7, fibroblast growth factor (FGF) 2, platelet-derived growth factor and TGF-β1 and TGF-β3 [207–216]. Growth factors, relevant to subchondral bone formation, include BMP-2, BMP-7, FGF-2 and IGF-1 [217–220]. Growth factors have a short half-life, therefore need to be regularly added to the culture environment, such as in the media, for in vitro or ex vivo culture [221]. Relying on growth factors in the culture environment presents a challenge when simultaneously aiming to stimulate cell(s) down different lineages in the one scaffold. To address this challenge, sophisticated culture conditions and bioreactors can be used, allowing different phases of the scaffold to be in direct contact with different medias and their associated growth factors [222,223]. Otherwise, the growth factors can be incorporated into the OC scaffold for sustained release either via passive release, triggered release or encapsulation (chemical or physical) [221]. Modulating the timing of this release as well as the crosstalk between layers is crucial. However, this mechanism has not been fully elucidated yet for use in tissue engineered strategies [224].

3.5. Elements of an OC Scaffold: Design

The design of an OC scaffold can be split into a mono, bi, tri or >triphasic design. In theory, a monophasic scaffold cannot capture the specific properties of each tissue, whereas multiphasic scaffolds were shown to replicate some of the properties of at least two of the three tissues by synergizing different combinations of materials, biological and/or mechanical elements in each phase (Figure 6). However, increasing the number of phases can also increase the complexity of fabrication and analysis. One extra category of design is a gradient scaffold, where each phase blends into one another rather than a distinct separation [225]. This is more difficult to achieve through nozzle-based fabrication as a filament or material reservoir is generally filled with a homogenous material, and the changing of materials requires the switching of reservoirs which creates a distinct separation between phases. As such, gradient scaffolds are not in the scope of this review.

Another consideration in the design of a 3D printed OC scaffold is the printed pattern of each layer. This pattern affects the interconnectivity of pores as well as overall porosity. Creating this desired pattern can be limited by the capabilities of the fabrication technique. As reported, fully interconnected, porous scaffolds facilitate cell migration through the entire construct, the diffusion of nutrients and removal of waste [226,227].

3.5.1. Monophasic Scaffold

A monophasic scaffold (Figure 7A) relies on the homogeneous design and material (or material composite) to repair the entire OC defect. This translates to a single porosity and mechanical property of the scaffold required to withstand the relevant forces in each tissue region. However, the ability to repair different tissues in an OC defect using a monophasic scaffold is challenging. Monophasic OC scaffolds have been created using a range of materials and biofabrication techniques, including ES of zinc oxide-PCL composite and ME of bioceramic [196,228]. In both cases, either concentrations or surface features were altered in order achieve enhanced chondrogenic or osteogenic potential, but the monophasic scaffolds on their own cannot achieve both.
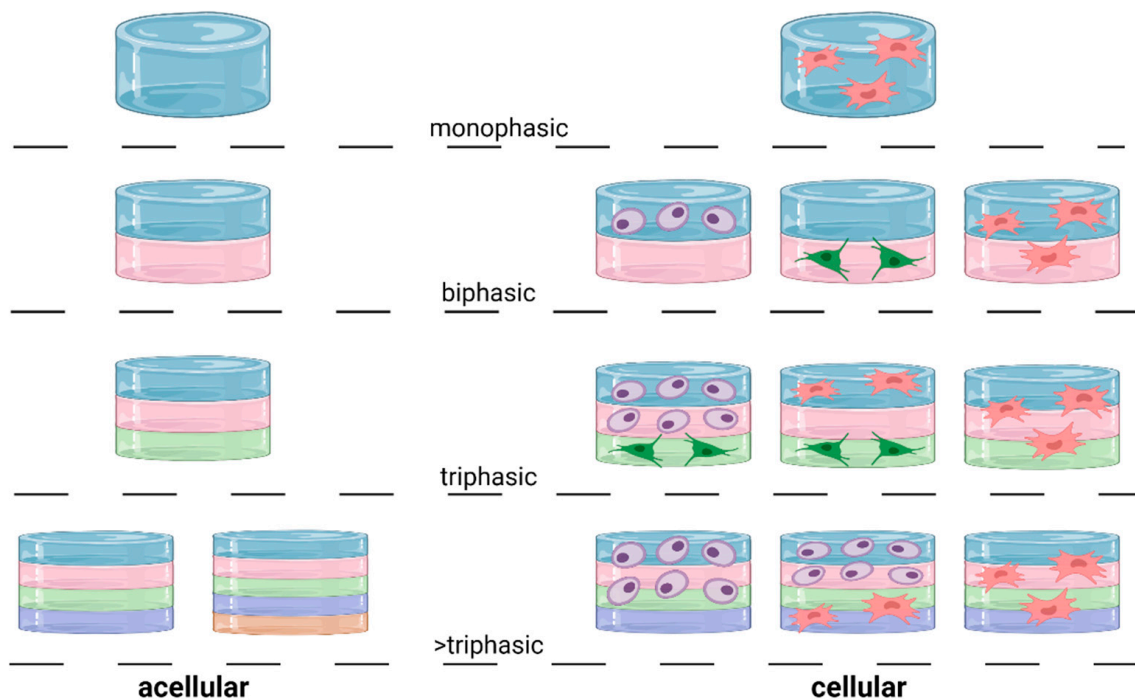
Figure 6. Design options for an OC scaffold. Categories include mono (one) phase, bi (two) phases, tri (three) phases and >tri (more than three phases). Any combination of number of phases, materials, and cell type can be used to create the 'ideal' OC scaffold. For example, chondrocytes (purple) are commonly used in the cartilage phase/s, osteoblasts (green) in the subchondral bone phase/s while MSCs (pink) are used throughout the whole OC scaffold. Figure created with BioRender.com (10 October 21).
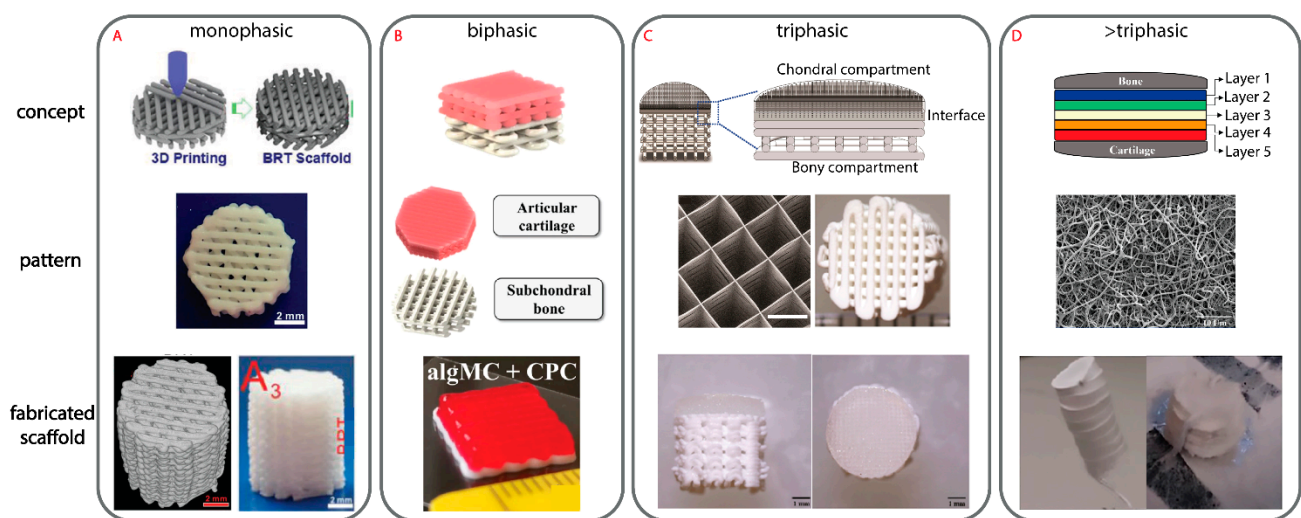

Figure 7. Examples of different scaffold design approaches including the pattern of each 3D printed layer. (**A**) A monophasic scaffold made from a homogenous ceramic paste ME printed. The text in the fabricated scaffold image is from the original research output [196]. (**B**) A biphasic scaffold with both phases ME printed. The subchondral bone phase is made from a ceramic paste and the cartilage phase is made from a hydrogel [109]. (**C**) A triphasic scaffold made from ME and MEW where the subchondral bone phase is made from a ceramic paste, the cartilage phase contains a thermopolymer MEW mesh and hydrogel while the interface contains all the forementioned materials [105]. (**D**) A >triphasic scaffold has more than three distinct phases with this example scaffold containing five individual phases all made from ES [165].

3.5.2. Biphasic Scaffold

Here, a biphasic scaffold (Figure 7B) is referred to the targeted repair of the bone and cartilage phases, typically neglecting the calcified cartilage in-between. Splitting the

scaffold into two allows customization in one or more elements, i.e., the material, design, porosity, mechanical function and/or cell type. This gives a greater ability to more closely mimic the structure of the natural tissue and drive the formation of multiple new tissues.

Kilian et al., characterized various biphasic combinations of their acellular ceramic 'cement' and cellular alginate-based hydrogel or by combining the two materials aimed to address the calcified cartilage [109]. The 3D printed scaffolds were confined to a 0, 90° log pile design that could have been designed or a limitation of the printing technique in combination with the materials. The biphasic scaffold by Critchley et al., featured a ME printed PCL scaffolds with a standard 0, 90° log pile design [110]. While utilizing a range of cells throughout the construct, the biphasic scaffold was cultured in chondrogenic media, therefore placing emphasis on the cellular response in the cartilage phase over that of the bone phase [110]. Despite this, after 6 months of the scaffolds implanted in vivo in an OC defect in a goat, the team observed the production of hyaline-like articular cartilage in most animals, but inconsistent results in the quality of subchondral bone were produced [110].

3.5.3. Triphasic Scaffold

Developing a triphasic scaffold (Figure 7C) allows for the interface or calcified cartilage phase to also be prioritized. Key considerations in each phase of the scaffold include the material, design and which cells, if any, are used (Table 2).

Table 2. Triphasic OC scaffolds.

	Cartilage Phase	Calcified Cartilage Phase	Subchondral Bone Phase	Ref
Material	Methacrylated hyaluronan, isocynatoethyl acrylate−modified β−cyclodextrin, kartogenin	All materials found in cartilage and bone phase	HA, alendronate	[102]
Design	Homogenously casted hydrogel	0°, 90° log pile infiltrated with homogenously casted hydrogel	0°, 90° logpile	
Cells	Human bmMSCs *	bmMSCs *	Human bmMSCs *	
Material	Cartilage ECM, chitosan	PLGA, TCP	PLGA, TCP	[121]
Design	Orientated casted hydrogel	0°, 90° log pile however ≈ 50 μm spacing between fibers so practically close to a solid disk	0°, 90° logpile	
Cells	Goat bmMSCs	Acellular	Goat bmMSCs	
Material	Alginate, PLA	Alginate, GelMA, TCP,	PCL	[104]
Design	0°, 90° log pile	0°, 90° log pile	0°, 90° log pile	
Cells	Acellular	Acellular	Acellular	
Material	PCL, GelMA	PCL + all materials in cartilage phase	α-TCP, nano−HA, hydrogel (either unmodified or modified poloxamer)	[105]
Design	0°, 90° log pile PCL infiltrated with homogenously casted GelMA	0°, −0°, −90°, −90° log pile (cartilage phase) and 0°, 90° log pile (bone phase)	0°, −0°, −90°, −90° log pile	
Cells	Articular cartilage progenitor cells (ACPCs)	Acellular	Acellular	
Material	Sodium alginate	Sodium alginate, mesoporous bioactive glasses	Sodium alginate, mesoporous bioactive glasses	[107]
Design	0°, 90° log pile	Dense/solid phase	0°, 60° rotation steps	
Cells	Acellular	Acellular	Acellular	

* Cells were seeded/incorporated into the scaffold to assess cytocompatibility only and do not necessarily represent the whole/final strategy for repair.

3.5.4. Triphasic Scaffold

The final category of design is the most complex with a minimum of four distinct phases (>triphasic therefore more than three phases) in the OC scaffold (Figure 7D). While this approach is not widely used, moving from three to four or more phases usually results in the breakdown of the cartilage phases into its different zones.

Mancini et al., have presented an OC scaffold consisting of four distinct phases, with the aim of better capturing the zonal nature of articular cartilage [101,229]. The PCL scaffold with a 0°, 90° log pile pattern serves as the base with the porosity gradually decreasing to a solid layer to act as the interface region. The log pile PCL then continues to a 70% porosity along and a hydrogel containing equine MSCs. The PCL is then removed leaving only hydrogel and MSCs followed by the final phase, with again the same hydrogel but with ACPCs instead of MSCs. The rationale for a stronger focus on the cartilage repair was due to its distinct lack of intrinsic healing capability without a vasculature structure [229].

Further increasing the number of phases is work reported by Hejazi et al., where a five-phase electrospun OC scaffold was developed [165]. The five-phase scaffold is based off various combinations of PCL, gelatin, chitosan, PVA and nano-HA. The team created the OC scaffold in the relevant height for an OC defect (15 mm); however, with no full biological characterization of the scaffold, it is yet to be seen whether the scaffold with five phases offers a benefit over those with 2–4 phases [165].

A representative scaffold from each of the four categories of deigns can be seen in Figure 7.

4. Functional Evaluation: In Vitro and In Vivo

The response of the scaffold under physiological conditions needs to be evaluated and can be achieved by using an in vitro, ex vivo, in vivo (animal models) and in vivo (human) studies.

An in vitro model is a logical first experiment to test the response of the OC scaffold as it is the cheapest, lowest risk and fastest way to generate biological results (Table 3) [230–232].

Table 3. In vitro models for the analysis of OC scaffolds.

In Vitro					
Design	**Materials**	**Elastic Modulus**	**Degradation**	**Outcome**	**Ref**
Mono-phasic	Insulin, PLGA, polydopamine, PCL	Monophasic scaffold: 233.71 ± 7.57 MPa	N/A	Significant increase in cell number, alkaline phosphatase, glycosaminoglycan/protein and Alizarin Red after 7–14 days when MSCs and chondrocytes were seeded onto the scaffold. There was also significant increase in SOX-9, collagen I and aggrecan suggesting chondrogenic differentiation and RUNX-2, collagen II and osteocalcin suggesting osteogenic differentiation.	[190]
Biphasic	PLA, PCL, HA, chitosan, silk firoin	Cartilage phase: 1.01 ± 0.04 GPa Bone phase: 1.07 ± 0.16 GPa	$0.33 \pm 0.09\%$ after 30 days	Cell viability increased from $125.25 \pm 9.36\%$ to $308.28 \pm 7.88\%$ from day 1 to 14 respectively. The presence of HA and CS/SF increased cell proliferation.	[119]
Biphasic	P(NAGA-co-THMMA) hydrogels, β-TCP	Biphasic scaffold: 16–115 kPa	N/A	Significant increase in collagen II and aggrecan after 14 days. Significant increase in alkaline phosphatase, collagen I, osteocalcin and RUNX2 after 14 days cultured in non-osteogenic media.	[113]

Table 3. *Cont.*

		In Vitro			
Design	**Materials**	**Elastic Modulus**	**Degradation**	**Outcome**	**Ref**
Biphasic	PCL, HA, interleukin-4 GelMA	Biphasic scaffold: 73 ± 1 to 75 ± 3 MPa	$\approx 75\%$ weight loss in 8 weeks	The cartilage scaffold was anti-inflammatory and had an increase in cell number after 5 days. Increase in RUNX2 and Alizarin Red staining in subchondral phase compared to the control.	[103]
Multi-phasic	PCL, PVA gelation, chitosan, nano-HA,	Multiphasic scaffold: 6.2 ± 0.5 MPa (low strain) 70 ± 29 MPa (40% strain)	$\approx 35\%$ weight loss in 12 weeks	Increase in MSC cell number over 21 days. Greater cell density, proliferation, and migration in the subchondral bone phase over the cartilage.	[165]

An ex vivo model can be a powerful tool lying between that of in vitro and in vivo models, where tissue from a human or animal is used outside of its original environment. A practical use of this model in OC research is to create an artificial defect in a condyle plug to implant in the tissue engineered scaffold. This model is useful for studying the integration between the implant and native tissue. However, the sample can be more difficult to post-process and analyze given multiple materials/tissues of varying compositions. Despite the potential of the ex vivo model, to date it has been rarely used to study a 3D printed full OC scaffold and is more commonly used in chondral-only defects [233–238].

For in vivo models, small models, such as rabbits and mice, are used more often than large animals-largely due to the reduced costs; however, the structure of the OC tissue is closer to humans in large models, such as horses, sheep and pigs and therefore be more beneficial in the regulatory pathway [101,239–242]. In addition, some small animals, especially rabbits, have a self-healing capability which means results from these models can be misleading [241]. These animal models, especially large models, are often a pre-clinical requirement and can provide significant information in predicting the fate of the treatment in humans (Table 4).

Table 4. In vivo animals models for OC scaffolds.

		In Vivo (Animals)			
Animal	**Design**	**Materials**	**Duration**	**Outcome**	**Ref**
Rabbit	Monophasic	Self-assembling peptide hydrogel coated PCL	12 weeks	Coating with hydrogel reduces chondrocyte death rate, and enhanced cell growth. Highly improved hydrophilicity and biomimetic ECM structures. Promoted neobone and neocartilage regeneration.	[117]
Rabbit	Biphasic	mPEG-PCL, HA, glycidyl methacrylate-hyaluronic acid, TGF-β1	12 weeks	The empty control had neobone formation only while the scaffold group had neobone and neocarilage formation. Some scaffold remained in the defect.	[130]
Rat	Biphasic	P(NAGA-co-THMMA) hydrogels, β-TCP	12 weeks	In the subchondral bone phase there was a significant increase in the total volume of tissue regenerated and bone mineral density compared to the control group and there was strong staining for osteocalcin, collagen I and toluidine blue. Neocartilage formation was present in the cartilage region with strong staining for glycosaminoglycan, collagen II and toluidine blue.	[113]

<div align="center">**Table 4.** *Cont.*</div>

In Vivo (Animals)					
Animal	**Design**	**Materials**	**Duration**	**Outcome**	**Ref**
Rabbit	Biphasic	PCL, HA, interleukin-4 GelMA	16 weeks	In the subchondral bone phase there was a significant increase in the total volume of tissue regenerated compared to the control group. Qualitative and quantitative Safranin O staining results were higher compared to the control.	[103]
Rabbit	Biphasic	β-TCP, PEG	12 months	By 12 months there was tissue formation the entire defect. In the subchondral bone phase there was a significant increase in the total volume of tissue regenerated at 24 weeks compared to the control.	[124]
Mini-pigs	Biphasic	mPEG-PCL, HA, glycidyl methacrylate-hyaluronic acid, TGF-β1	12 months	Scaffold was still present in the subchondral bone phase while the cartilage phase was taken over by semi-mature cartilage. The subchondral bone phase also contained mixed bone and fibrotic tissue Of note: the control defect was completely filled but with fibrocartilage.	[243]

Human in vivo experiments or clinical trials are the ultimate model to achieve clinical translation. However, the road to human clinical trials is long with rigorous ethical, legal and documentation checkpoints as well as high costs. Unlike the previous models, an OC scaffold implant cannot be removed after a specific time period and instead, techniques including MRI and patient questionnaires are used. According to the Clinical Trials database by the U.S. National Library of Medicine (search was based on using the keywords 'osteochondral' and '3D print'), there are currently no clinical trials (underway, completed or recruiting) related to 3D printed scaffolds for OC repair in the knee. However, there have been a limited number of clinical trials related to tissue engineering OC scaffolds, not fabricated by 3D printing, including (i) ChondroMimetic, a biphasic scaffold with a cartilage phase made of collagen and GAG and a bone phase also made of collagen and GAG plus calcium phosphate (study completed); (ii) Agili-C™, a porous, resorbable biphasic scaffold, containing calcium carbonate (study completed) and BioMatrix CRD, a biphasic, bioresorbable scaffold containing collagen in the cartilage phase and TCP in the bone layer (study completed).

All the evaluation stages, from non-clinical, i.e., in vitro and animal models, to clinical trials are aligned with the regulatory framework established for medical devices [242].

5. Discussion and Future Outlooks

This review discusses in detail the approaches to creating scaffolds for the repair of the entire OC tissue, including the subchondral bone, articular cartilage and the calcified cartilage in between. We have presented five main areas of consideration when creating an OC scaffold, i.e., material, fabrication method, mechanical function, biological components and design. Each of these five requirements for creating the OC scaffold are heavily interconnected.

Considerations for the material include its physical properties, printability, biological response and inherit mechanical properties. Some of these properties, such as printability, may be enhanced through substantial optimization of the printing parameters or modification of the material [244]. Included in the multiphasic scaffold method, is a multi-material approach which offers the ability to carefully select the material for each specific region of the scaffold to elicit the desired response. While no single material has been proven to be superior to their counterparts, bioceramics, including HA and TCP, are specific to the subchondral bone phase, while hydrogels are becoming the material of choice for the cartilage phase. In current approaches, the interface region is often only a combination of the materials used in the cartilage and subchondral phase. This shows that the cal-

cified cartilage is not understood as well as its adjacent tissues (articular cartilage and subchondral bone).

In more than 80 research studies, focused on developing 3D printed OC scaffolds and included in this review, ME printing was the most commonly used fabrication technique. This is likely due to ME printing's wide availability, material versatility and low cost. While MEW and ES are still popular choices, they are primarily used for the cartilage phase only, and their traditional print style limits the achievable scaffold thickness. This results in the necessity of stacking many scaffolds or sheets aiming to reach a relevant or desired thickness. The use and choice of a fabrication method should not be underestimated as it primarily controls critical scaffold design parameters, such as pore size and porosity, which can facilitate tissue ingrowth. Using a combination of 3D printing techniques is common in the literature and offers a promising approach to better capture the varying tissue regions, especially in terms of mechanical functionality [105].

While there is evidence to suggest that the mechanical function of a biological implant should be close to that of the native tissue, there are still many research outputs that do not prioritize the mechanical characterization of their scaffolds [245–247]. Overall, compressive-based measurements featured more often than tensile or shear stress tests in the literature, suggesting that when the forces on the condyles of the knee are simplified, compression is seen to be dominant. The true importance of the mechanical function is likely not to be seen until long-term in vivo studies with a large-scale animal model are conducted, where the movement and effect of load-bearing is more similar to that of humans.

The element of design provides an insight to where the field is heading, with a continued emphasis on multiphasic scaffolds. Increasing the number of phases in a scaffold provides the ability to tailor each region to the specific tissue rather than trying to repair three tissues with a single material, pattern and/or cell type. Further into the overall design is the pattern of each 3D printed layer driven by the capabilities of the fabrication technique with a given material. The 0, 90° log pile continues to be the most common pattern in 3D printed OC scaffolds. This represents a limitation in nozzle-based fabrication, where each layer needs to be at least partially supported by itself or a support material in order to create a 3D structure [144]. While a 0, 90° log pile pattern can produce an overall interconnected scaffold, if there is good definition (i.e., fibers do not sag thereby touching the layers below) in each layer, alternative designs, including lattice structures, can offer a greater freedom in design pattern, porosity and mechanical function but are not commonly used in nozzle-based fabrication. While SLA approaches can circumvent this design limitation, there is little demonstration of this with OC scaffolds [123,125,181,248]. This offers a significant opportunity for future research in developing OC scaffolds.

The fully fabricated scaffold needs to be evaluated to test the combination of the core elements via biological characterization, including in vitro, ex vivo, in vivo (animal) and in vivo (human)/clinical trials. In this order the model increases in complexity, cost, resources and time of experiments but also represents a logical progression in the translation from bench to clinic. The ex vivo model offers an opportunity to study the integration of the OC scaffold with the native tissue, thus presenting another research direction in developing advanced OC scaffolds.

Finally, a significant challenge to address is the lack of standardization. This extends to the terminology used, type of mechanical test performed, output presented, biological characterization and markers used, etc. While the lack of standardization is common across all areas of tissue engineering, it makes it difficult to conclude which OC scaffold in the research stage is the most promising for translation to clinic. This is especially evident in the mechanical function, since despite the OC defect occurring in a weight bearing region, not all research outputs include any mechanical data nor discuss the implication on the design and function of the developed scaffold. Furthermore, even when there are shared targets between research studies, such as matching the mechanical function of the scaffold to the native tissue, that native tissue target can still vary depending on various factors, including if the target values are from native animal or human tissue, diseased or healthy

tissue, type of test and test conditions etc. One way to help overcome this limitation could be to employ a streamlined mechanical protocol, like that produced by Kabir et al., which allows for the sequential testing of a single sample to generate many key pieces of relevant mechanical data rather than only one or two [33].

It is widely reported that the current surgical approaches for repairing an OC defect still have significant drawbacks, therefore a 3D printed multiphasic scaffold approach offers the potential to achieve a superior result by repairing each of the native tissues in the OC unit. The full capabilities of 3D printing are currently underutilized and thus, present an area for potential improvement in the design capabilities and biomimicry of the printed scaffolds. While there is no single material or fabrication method that has proven to be superior in developing an OC scaffold, a multiphasic scaffold seems to be the best approach to creating tailored environments to regrow each of the elements within the OC unit. The calcified cartilage region remains the least understood region in the tissue engineered scaffold, as such, the role of this region needs to be better defined and addressed. However, the strong focus on biofabricated multiphasic scaffolds provides an optimistic outlook to developing a method for full repair of the OC function and its further translation to an improved clinical treatment and patient outcome.

Abbreviations

OC	Osteochondral
OAT	Osteochondral Autograft Transfer
OCA	Osteochondral Allograft Transplant
PLA	Polylactic Acid
PCL	Polycaprolactone
PLGA	Poly(L-lactic-co-Glycolic Acid)
PEG	Polyethylene Glycol
PVA	Polyvinyl Alcohol
ECM	Extracellular Matrix
HA	Hydroxyapatite
TCP	Tricalcium Phosphate
ME	Material Extrusion
MEW	Melt Electro-Writing
ES	Electro-Spinning
SLA	Stereolithography
DLP	Digital Light Processing
MSC	Mesenchymal Stem/Stromal Cell
bmMSC	Bone Marrow derived Mesenchymal Stem/Stromal Cell
ACPC	Articular Cartilage Progenitor Cell
IGF	Insulin-like Growth Factor

BMP	Bone Morphogenetic Proteins
FGF	Fibroblast Growth Factor
TGF	Transforming Growth Factor

References

1. Hall, S. *ISE EBook Online Access for Basic Biomechanics*; McGraw-Hill Higher Education: New York, NY, USA, 2021; ISBN 9781264363674.
2. Sophia Fox, A.J.; Bedi, A.; Rodeo, S.A. The basic science of articular cartilage: Structure, composition, and function. *Sports Health* **2009**, *1*, 461–468. [CrossRef] [PubMed]
3. Gomoll, A.H.; Minas, T. The quality of healing: Articular cartilage. *Wound Repair Regen.* **2014**, *22*, 30–38. [CrossRef]
4. Giffin, J.R.; Annunziata, C.C.; Vogrin, T.M.; Harner, C.D. Primary repair of osteochondral and chondral injury. *Oper. Tech. Orthop.* **2001**, *11*, 83–89. [CrossRef]
5. Steinert, A.F.; Nöth, U.; Tuan, R.S. Concepts in gene therapy for cartilage repair. *Injury* **2008**, *39*, 97–113. [CrossRef]
6. Ebihara, G.; Sato, M.; Yamato, M.; Mitani, G.; Kutsuna, T.; Nagai, T.; Ito, S.; Ukai, T.; Kobayashi, M.; Kokubo, M.; et al. Cartilage repair in transplanted scaffold-free chondrocyte sheets using a minipig model. *Biomaterials* **2012**, *33*, 3846–3851. [CrossRef]
7. Hunziker, E.B. Articular cartilage repair: Basic science and clinical progress. A review of the current status and prospects. *Osteoarthr. Cartil.* **2002**, *10*, 432–463. [CrossRef]
8. Armiento, A.R.; Alini, M.; Stoddart, M.J. Articular fibrocartilage-Why does hyaline cartilage fail to repair? *Adv. Drug Deliv. Rev.* **2019**, *146*, 289–305. [CrossRef] [PubMed]
9. Huey, D.J.; Hu, J.C.; Athanasiou, K.A. Unlike bone, cartilage regeneration remains elusive. *Science* **2012**, *338*, 917–921. [CrossRef]
10. Outerbridge, R.E. The etiology of chondromalacia patellae. *J. Bone Joint Surg. Br.* **1961**, *43*, 752–757. [CrossRef] [PubMed]
11. Tetteh, E.S.; Bajaj, S.; Ghodadra, N.S.; Cole, B.J. Basic science and surgical treatment options for articular cartilage injuries of the knee. *J. Orthop. Sports Phys. Ther.* **2012**, *42*, 243–253. [CrossRef] [PubMed]
12. Widuchowski, W.; Widuchowski, J.; Trzaska, T. Articular cartilage defects: Study of 25,124 knee arthroscopies. *Knee* **2007**, *14*, 177–182. [CrossRef] [PubMed]
13. Anderson, D.E.; Rose, M.B.; Wille, A.J.; Wiedrick, J.; Crawford, D.C. Arthroscopic Mechanical Chondroplasty of the Knee Is Beneficial for Treatment of Focal Cartilage Lesions in the Absence of Concurrent Pathology. *Orthop. J. Sport. Med.* **2017**, *5*, 5. [CrossRef]
14. Curl, W.W.; Krome, J.; Gordon, E.S.; Rushing, J.; Smith, B.P.; Poehling, G.G. Cartilage injuries: A review of 31,516 knee arthroscopies. *Arthrosc. J. Arthrosc. Relat. Surg.* **1997**, *13*, 456–460. [CrossRef]
15. Beris, A.E.; Lykissas, M.G.; Papageorgiou, C.D.; Georgoulis, A.D. Advances in articular cartilage repair. *Injury* **2005**, *36* (Suppl. S4), S14–S23. [CrossRef]
16. Guettler, J.H.; Demetropoulos, C.K.; Yang, K.H.; Jurist, K.A. Osteochondral defects in the human knee: Influence of defect size on cartilage rim stress and load redistribution to surrounding cartilage. *Am. J. Sports Med.* **2004**, *32*, 1451–1458. [CrossRef] [PubMed]
17. Salzmann, G.M.; Niemeyer, P.; Hochrein, A.; Stoddart, M.J.; Angele, P. Articular Cartilage Repair of the Knee in Children and Adolescents. *Orthop. J. Sport. Med.* **2018**, *6*, 3. [CrossRef] [PubMed]
18. Burns, T.C.; Giuliani, J.R.; Svoboda, S.J.; Owens, B.D. Knee Cartilage Tibio-Femoral Injuries. *Tech. Orthop.* **2010**, *25*, 208–216. [CrossRef]
19. Lepage, S.I.M.; Robson, N.; Gilmore, H.; Davis, O.; Hooper, A.; St John, S.; Kamesan, V.; Gelis, P.; Carvajal, D.; Hurtig, M.; et al. Beyond Cartilage Repair: The Role of the Osteochondral Unit in Joint Health and Disease. *Tissue Eng. Part B Rev.* **2019**, *25*, 114–125. [CrossRef] [PubMed]
20. Ricci, M.; Tradati, D.; Maione, A.; Uboldi, F.M.; Usellini, E.; Berruto, M. Cell-free osteochondral scaffolds provide a substantial clinical benefit in the treatment of osteochondral defects at a minimum follow-up of 5 years. *J. Exp. Orthop.* **2021**, *8*, 62. [CrossRef]
21. Langer, R.; Vacanti, J.P. Tissue engineering. *Science* **1993**, *260*, 920. [CrossRef]
22. Abdollahiyan, P.; Oroojalian, F.; Mokhtarzadeh, A.; de la Guardia, M. Hydrogel-Based 3D Bioprinting for Bone and Cartilage Tissue Engineering. *Biotechnol. J.* **2020**, *15*, 12. [CrossRef]
23. Harley, W.S.; Li, C.C.; Toombs, J.; O'Connell, C.D.; Taylor, H.K.; Heath, D.E.; Collins, D.J. Advances in biofabrication techniques towards functional bioprinted heterogeneous engineered tissues: A comprehensive review. *Bioprinting* **2021**, *23*, e00147. [CrossRef]
24. Groll, J.; Boland, T.; Blunk, T.; Burdick, J.A.; Cho, D.-W.; Dalton, P.D.; Derby, B.; Forgacs, G.; Li, Q.; Mironov, V.A.; et al. Biofabrication: Reappraising the definition of an evolving field. *Biofabrication* **2016**, *8*, 13001. [CrossRef] [PubMed]
25. Viola, M.; Piluso, S.; Groll, J.; Vermonden, T.; Malda, J.; Castilho, M. The Importance of Interfaces in Multi-Material Biofabricated Tissue Structures. *Adv. Healthc. Mater.* **2021**, *10*, 2101021. [CrossRef]
26. Lim, K.S.; Levato, R.; Costa, P.F.; Castilho, M.D.; Alcala-Orozco, C.R.; van Dorenmalen, K.M.A.; Melchels, F.P.W.; Gawlitta, D.; Hooper, G.J.; Malda, J.; et al. Bio-resin for high resolution lithography-based biofabrication of complex cell-laden constructs. *Biofabrication* **2018**, *10*, 34101. [CrossRef] [PubMed]
27. Abdulghani, S.; Morouço, P.G. Biofabrication for osteochondral tissue regeneration: Bioink printability requirements. *J. Mater. Sci. Mater. Med.* **2019**, *30*, 20. [CrossRef]
28. Turnbull, G.; Clarke, J.; Picard, F.; Riches, P.; Jia, L.; Han, F.; Li, B.; Shu, W. 3D bioactive composite scaffolds for bone tissue engineering. *Bioact. Mater.* **2018**, *3*, 278–314. [CrossRef] [PubMed]

29. Athanasiou, K.A.; Darling, E.M.; Hu, J.C. *Articular Cartilage Tissue Engineering*; Morgan & Claypool Publishers: San Rafael, CA, USA, 2009; ISBN 9781598298758.

30. Lees, D.; Partington, P. Articular cartilage. *Orthop. Trauma* **2016**, *30*, 265–272. [CrossRef]

31. Correia, C.R.; Reis, R.L.; Mano, J.F. Multiphasic, Multistructured and Hierarchical Strategies for Cartilage Regeneration. In *Engineering Mineralized and Load Bearing Tissues*; Bertassoni, L.E., Coelho, P.G., Eds.; Springer International Publishing: Cham, Switzerland, 2015; pp. 143–160. ISBN 978-3-319-22345-2.

32. Vyas, C.; Poologasundarampillai, G.; Hoyland, J.; Bartolo, P. 12-3D printing of biocomposites for osteochondral tissue engineering. In *Biomedical Composites*; Woodhead Publishing: Sawston, UK, 2017; pp. 261–302. ISBN 978-0-08-100752-5.

33. Kabir, W.; Di Bella, C.; Choong, P.F.M.; O'Connell, C.D. Assessment of Native Human Articular Cartilage: A Biomechanical Protocol. *Cartilage* **2020**, 1–11. [CrossRef]

34. Jurvelin, J.S.; Buschmann, M.D.; Hunziker, E.B. Mechanical anisotropy of the human knee articular cartilage in compression. *Proc. Inst. Mech. Eng. Part H J. Eng. Med.* **2003**, *217*, 215–219. [CrossRef]

35. Kiviranta, P.; Lammentausta, E.; Töyräs, J.; Kiviranta, I.; Jurvelin, J.S. Indentation diagnostics of cartilage degeneration. *Osteoarthr. Cartil.* **2008**, *16*, 796–804. [CrossRef]

36. Antons, J.; Marascio, M.G.M.; Nohava, J.; Martin, R.; Applegate, L.A.; Bourban, P.E.; Pioletti, D.P. Zone-dependent mechanical properties of human articular cartilage obtained by indentation measurements. *J. Mater. Sci. Mater. Med.* **2018**, *29*, 57. [CrossRef]

37. Renault, J.-B.; Carmona, M.; Tzioupis, C.; Ollivier, M.; Argenson, J.-N.; Parratte, S.; Chabrand, P. Tibial subchondral trabecular bone micromechanical and microarchitectural properties are affected by alignment and osteoarthritis stage. *Sci. Rep.* **2020**, *10*, 3975. [CrossRef] [PubMed]

38. Ding, M.; Danielsen, C.C.; Hvid, I. Bone density does not reflect mechanical properties in early-stage arthrosis. *Acta Orthop. Scand.* **2001**, *72*, 181–185. [CrossRef]

39. Day, J.S.; Ding, M.; van der Linden, J.C.; Hvid, I.; Sumner, D.R.; Weinans, H. A decreased subchondral trabecular bone tissue elastic modulus is associated with pre-arthritic cartilage damage. *J. Orthop. Res.* **2001**, *19*, 914–918. [CrossRef]

40. Chen, Y.; Huang, Y.-C.; Yan, C.H.; Chiu, K.Y.; Wei, Q.; Zhao, J.; Guo, X.E.; Leung, F.; Lu, W.W. Abnormal subchondral bone remodeling and its association with articular cartilage degradation in knees of type 2 diabetes patients. *Bone Res.* **2017**, *5*, 17034. [CrossRef]

41. Hunziker, E.B.; Quinn, T.M.; Häuselmann, H.-J. Quantitative structural organization of normal adult human articular cartilage. *Osteoarthr. Cartil.* **2002**, *10*, 564–572. [CrossRef]

42. Mow, V.C.; Holmes, M.H.; Lai, W.M. Fluid transport and mechanical properties of articular cartilage: A review. *J. Biomech.* **1984**, *17*, 377–394. [CrossRef]

43. Thonar, E.J.-M.A.; Masuda, K.; Manicourt, D.H.; Kuettner, K.E. Structure and Function of Normal Human Adult Articular Cartilage. In *Osteoarthritis: Clinical and Experimental Aspects*; Reginster, J.-Y., Pelletier, J.-P., Martel-Pelletier, J., Henrotin, Y., Crasborn, L., Eds.; Springer: Berlin/Heidelberg, Germany, 1999; pp. 1–19. ISBN 978-3-642-60026-5.

44. Mansfield, J.C.; Bell, J.S.; Winlove, C.P. The micromechanics of the superficial zone of articular cartilage. *Osteoarthr. Cartil.* **2015**, *23*, 1806–1816. [CrossRef] [PubMed]

45. Eschweiler, J.; Horn, N.; Rath, B.; Betsch, M.; Baroncini, A.; Tingart, M.; Migliorini, F. The Biomechanics of Cartilage-An Overview. *Life* **2021**, *11*, 302. [CrossRef]

46. Han, S.-K.; Federico, S.; Grillo, A.; Giaquinta, G.; Herzog, W. The Mechanical Behaviour of Chondrocytes Predicted with a Micro-structural Model of Articular Cartilage. *Biomech. Model. Mechanobiol.* **2007**, *6*, 139–150. [CrossRef] [PubMed]

47. Setton, L.A.; Elliott, D.M.; Mow, V.C. Altered mechanics of cartilage with osteoarthritis: Human osteoarthritis and an experimental model of joint degeneration. *Osteoarthr. Cartil.* **1999**, *7*, 2–14. [CrossRef]

48. Decker, R.S.; Koyama, E.; Pacifici, M. Articular Cartilage: Structural and Developmental Intricacies and Questions. *Curr. Osteoporos. Rep.* **2015**, *13*, 407–414. [CrossRef]

49. Gilbert, S.J.; Blain, E.J. Chapter 4-Cartilage Mechanobiology: How Chondrocytes Respond to Mechanical Load. In *Mechanobiology in Health and Disease*; Verbruggen, S., Ed.; Academic Press: Cambridge, MA, USA, 2018; pp. 99–126. ISBN 978-0-12-812952-4.

50. Sefat, F.; Raja, T.I.; Zafar, M.S.; Khurshid, Z.; Najeeb, S.; Zohaib, S.; Ahmadi, E.D.; Rahmati, M.; Mozafari, M. Chapter 3-Nanoengineered Biomaterials for Cartilage Repair. In *Nanoengineered Biomaterials for Regenerative Medicine*; Mozafari, M., Rajadas, J., Kaplan, D., Eds.; Elsevier: Amsterdam, The Netherlands, 2019; pp. 39–71. ISBN 978-0-12-813355-2.

51. Xia, Y.; Momot, K.; Chen, Z.; Chen, C.; Kahn, D.; Badar, F. Introduction to Cartilage. In *Biophysics and Biochemistry of Cartilage by NMR and MRI*; Royal Society of Chemistry: London, UK, 2016; pp. 1–43. ISBN 978-1-78262-133-1.

52. Fan, X.; Wu, X.; Crawford, R.; Xiao, Y.; Prasadam, I. Macro, Micro, and Molecular. Changes of the Osteochondral Interface in Osteoarthritis Development. *Front. Cell Dev. Biol.* **2021**, *9*, 1148. [CrossRef] [PubMed]

53. Ansari, S.; Khorshidi, S.; Karkhaneh, A. Engineering of gradient osteochondral tissue: From nature to lab. *Acta Biomater.* **2019**, *87*, 41–54. [CrossRef]

54. Bhosale, A.M.; Richardson, J.B. Articular cartilage: Structure, injuries and review of management. *Br. Med. Bull.* **2008**, *87*, 77–95. [CrossRef] [PubMed]

55. Poole, A.R.; Kojima, T.; Yasuda, T.; Mwale, F.; Kobayashi, M.; Laverty, S. Composition and structure of articular cartilage: A template for tissue repair. *Clin. Orthop. Relat. Res.* **2001**, *391*, S26–S33. [CrossRef] [PubMed]

56. He, B.; Wu, J.P.; Kirk, T.B.; Carrino, J.A.; Xiang, C.; Xu, J. High-resolution measurements of the multilayer ultra-structure of articular cartilage and their translational potential. *Arthritis Res. Ther.* **2014**, *16*, 205. [CrossRef] [PubMed]

57. Nukavarapu, S.P.; Dorcemus, D.L. Osteochondral tissue engineering: Current strategies and challenges. *Biotechnol. Adv.* **2013**, *31*, 706–721. [CrossRef] [PubMed]

58. Zhang, Y.; Wang, F.; Tan, H.; Chen, G.; Guo, L.; Yang, L. Analysis of the Mineral Composition of the Human Calcified Cartilage Zone. *Int. J. Med. Sci.* **2012**, *9*, 353–360. [CrossRef] [PubMed]

59. Stewart, H.; Kawcak, C. The Importance of Subchondral Bone in the Pathophysiology of Osteoarthritis. *Front. Vet. Sci.* **2018**, *5*, 178. [CrossRef]

60. Kawcak, C.E.; McIlwraith, C.W.; Norrdin, R.W.; Park, R.D.; James, S.P. The role of subchondral bone in joint disease: A review. *Equine Vet. J.* **2001**, *33*, 120–126. [CrossRef]

61. Becerra, J.; Andrades, J.A.; Guerado, E.; Zamora-Navas, P.; López-Puertas, J.M.; Reddi, A.H. Articular Cartilage: Structure and Regeneration. *Tissue Eng. Part B Rev.* **2010**, *16*, 617–627. [CrossRef]

62. Bonewald, L.F. Chapter 313-Cell–Cell and Cell–Matrix Interactions in Bone. In *Handbook of Cell Signaling*; Bradshaw, R.A., Dennis, E.A., Eds.; Academic Press: San Diego, CA, USA, 2010; pp. 2647–2662. ISBN 978-0-12-374145-5.

63. Di Luca, A.; Van Blitterswijk, C.; Moroni, L. The osteochondral interface as a gradient tissue: From development to the fabrication of gradient scaffolds for regenerative medicine. *Birth Defects Res. C Embryo Today* **2015**, *105*, 34–52. [CrossRef]

64. Madry, H.; van Dijk, C.N.; Mueller-Gerbl, M. The basic science of the subchondral bone. *Knee Surg. Sports Traumatol. Arthrosc.* **2010**, *18*, 419–433. [CrossRef]

65. Magill, P.; Byrne, D.P.; Baker, J.F.; Mulhall, K.J. Review Article: Osteochondral Reconstruction and Grafting. *J. Orthop. Surg.* **2011**, *19*, 93–98. [CrossRef]

66. Gracitelli, G.C.; Moraes, V.Y.; Franciozi, C.E.; Luzo, M.V.; Belloti, J.C. Surgical interventions (microfracture, drilling, mosaicplasty, and allograft transplantation) for treating isolated cartilage defects of the knee in adults. *Cochrane Database Syst. Rev.* **2016**, *9*, CD010675. [CrossRef] [PubMed]

67. Mirza, M.Z.; Swenson, R.D.; Lynch, S.A. Knee cartilage defect: Marrow stimulating techniques. *Curr. Rev. Musculoskelet. Med.* **2015**, *8*, 451–456. [CrossRef] [PubMed]

68. Vogt, S.; Angele, P.; Arnold, M.; Brehme, K.; Cotic, M.; Haasper, C.; Hinterwimmer, S.; Imhoff, A.B.; Petersen, W.; Salzmann, G.; et al. Practice in rehabilitation after cartilage therapy: An expert survey. *Arch. Orthop. Trauma Surg.* **2013**, *133*, 311–320. [CrossRef]

69. Steadman, J.R.; Rodkey, W.G.; Briggs, K.K. Microfracture: Its History and Experience of the Developing Surgeon. *Cartilage* **2010**, *1*, 78–86. [CrossRef] [PubMed]

70. Steadman, J.R.; Rodkey, W.G.; Singleton, S.B.; Briggs, K.K. Microfracture technique forfull-thickness chondral defects: Technique and clinical results. *Oper. Tech. Orthop.* **1997**, *7*, 300–304. [CrossRef]

71. Bader, S.; Miniaci, A. Mosaïcplasty. *Orthopedics* **2011**, *34*, e491–e493. [CrossRef] [PubMed]

72. Robert, H. Chondral repair of the knee joint using mosaicplasty. *Orthop. Traumatol. Surg. Res.* **2011**, *97*, 418–429. [CrossRef] [PubMed]

73. Robinson, P.G.; Williamson, T.; Murray, I.R.; Al-Hourani, K.; White, T.O. Sporting participation following the operative management of chondral defects of the knee at mid-term follow up: A systematic review and meta-analysis. *J. Exp. Orthop.* **2020**, *7*, 76. [CrossRef] [PubMed]

74. Rowland, R.; Colello, M.; Wyland, D.J. Osteochondral Autograft Transfer Procedure: Arthroscopic Technique and Technical Pearls. *Arthrosc. Tech.* **2019**, *8*, e713–e719. [CrossRef] [PubMed]

75. Shekhar, A.; Reddy, S.; Patil, S.; Tapasvi, S. Mid-term outcomes of arthroscopic osteochondral autograft transplantation for focal chondral defects of the knee. *J. Arthrosc. Surg. Sport. Med.* **2021**, *2*, 41–46. [CrossRef]

76. Pareek, A.; Reardon, P.; Maak, T.; Levy, B.; Stuart, M.; Krych, A. Long-term Outcomes After Osteochondral Autograft Transfer: A Systematic Review at Mean Follow-up of 10.2 Years. *Arthrosc. J. Arthrosc. Relat. Surg.* **2016**, *32*, 1174–1184. [CrossRef]

77. Ma, H.-L.; Hung, S.-C.; Wang, S.-T.; Chang, M.-C.; Chen, T.-H. Osteochondral autografts transfer for post-traumatic osteochondral defect of the knee-2 to 5 years follow-up. *Injury* **2004**, *35*, 1286–1292. [CrossRef] [PubMed]

78. Hangody, L.; Fules, P. Autologous osteochondral mosaicplasty for the treatment of full-thickness defects of weight-bearing joints: Ten years of experimental and clinical experience. *J. Bone Jt. Surg.* **2003**, *85*, 25–32. [CrossRef]

79. Stone, A.V.; Christian, D.R.; Redondo, M.L.; Yanke, A.B.; Southworth, T.M.; Tauro, T.M.; Cole, B.J. Osteochondral Allograft Transplantation and Osteochondral Autograft Transfer. *Oper. Tech. Sports Med.* **2018**, *26*, 183–188. [CrossRef]

80. Richter, D.L.; Schenck, R.C.J.; Wascher, D.C.; Treme, G. Knee Articular Cartilage Repair and Restoration Techniques: A Review of the Literature. *Sports Health* **2016**, *8*, 153–160. [CrossRef]

81. Solheim, E.; Hegna, J.; Øyen, J.; Harlem, T.; Strand, T. Results at 10 to 14 years after osteochondral autografting (mosaicplasty) in articular cartilage defects in the knee. *Knee* **2013**, *20*, 287–290. [CrossRef] [PubMed]

82. Trengove, A.; Di Bella, C.; O'Connor, A.J. The Challenge of Cartilage Integration: Understanding a Major Barrier to Chondral Repair. *Tissue Eng. Part B. Rev.* **2021**, ahead of print. [CrossRef] [PubMed]

83. Karim, A.; Hall, A.C. Hyperosmolarity normalises serum-induced changes to chondrocyte properties in a model of cartilage injury. *Eur. Cells Mater.* **2016**, *31*, 205–220. [CrossRef]

84. Wang, D.; Chang, B.; Coxe, F.R.; Pais, M.D.; Wickiewicz, T.L.; Warren, R.F.; Rodeo, S.A.; Williams, R.J. 3rd Clinically Meaningful Improvement After Treatment of Cartilage Defects of the Knee With Osteochondral Grafts. *Am. J. Sports Med.* **2019**, *47*, 71–81. [CrossRef] [PubMed]

85. Assenmacher, A.T.; Pareek, A.; Reardon, P.J.; Macalena, J.A.; Stuart, M.J.; Krych, A.J. Long-term Outcomes After Osteochondral Allograft: A Systematic Review at Long-term Follow-up of 12.3 Years. *Arthrosc. J. Arthrosc. Relat. Surg.* **2016**, *32*, 2160–2168. [CrossRef] [PubMed]

86. Torrie, A.M.; Kesler, W.W.; Elkin, J.; Gallo, R.A. Osteochondral allograft. *Curr. Rev. Musculoskelet. Med.* **2015**, *8*, 413–422. [CrossRef]

87. Pearsall, A.W.; Madanagopal, S.G.; Hughey, J.T. Osteoarticular Autograft and Allograft Transplantation of the Knee: 3 year Follow-up. *Orthopedics* **2008**, *31*, 73.

88. Ye, K.; Di Bella, C.; Myers, D.E.; Choong, P.F.M. The osteochondral dilemma: Review of current management and future trends. *ANZ J. Surg.* **2014**, *84*, 211–217. [CrossRef]

89. Wang, K.C.; Frank, R.M.; Cotter, E.J.; Christian, D.R.; Cole, B.J. Arthroscopic Management of Isolated Tibial Plateau Defect With Microfracture and Micronized Allogeneic Cartilage–Platelet-Rich Plasma Adjunct. *Arthrosc. Tech.* **2017**, *6*, e1613–e1618. [CrossRef]

90. Ghassemi, T.; Shahroodi, A.; Ebrahimzadeh, M.H.; Mousavian, A.; Movaffagh, J.; Moradi, A. Current Concepts in Scaffolding for Bone Tissue Engineering. *Arch. Bone Jt. Surg.* **2018**, *6*, 90–99.

91. Koons, G.L.; Diba, M.; Mikos, A.G. Materials design for bone-tissue engineering. *Nat. Rev. Mater.* **2020**, *5*, 584–603. [CrossRef]

92. Ahmed, E.M. Hydrogel: Preparation, characterization, and applications: A review. *J. Adv. Res.* **2015**, *6*, 105–121. [CrossRef]

93. Sánchez-Téllez, D.A.; Téllez-Jurado, L.; Rodríguez-Lorenzo, L.M. Hydrogels for Cartilage Regeneration, from Polysaccharides to Hybrids. *Polymers* **2017**, *9*, 671. [CrossRef]

94. Zhu, J.; Marchant, R.E. Design properties of hydrogel tissue-engineering scaffolds. *Expert Rev. Med. Devices* **2011**, *8*, 607–626. [CrossRef]

95. Fuchs, S.; Shariati, K.; Ma, M. Specialty Tough Hydrogels and Their Biomedical Applications. *Adv. Healthc. Mater.* **2020**, *9*, e1901396. [CrossRef] [PubMed]

96. Gao, F.; Xu, Z.; Liang, Q.; Li, H.; Peng, L.; Wu, M.; Zhao, X.; Cui, X.; Ruan, C.; Liu, W. Osteochondral Regeneration with 3D-Printed Biodegradable High-Strength Supramolecular Polymer Reinforced-Gelatin Hydrogel Scaffolds. *Adv. Sci.* **2019**, *6*, 1900867. [CrossRef]

97. Liu, J.; Li, L.; Suo, H.; Yan, M.; Yin, J.; Fu, J. 3D printing of biomimetic multi-layered GelMA/nHA scaffold for osteochondral defect repair. *Mater. Des.* **2019**, *171*, 107708. [CrossRef]

98. Shim, J.-H.; Jang, K.-M.; Hahn, S.K.; Park, J.Y.; Jung, H.; Oh, K.; Park, K.M.; Yeom, J.; Park, S.H.; Kim, S.W.; et al. Three-dimensional bioprinting of multilayered constructs containing human mesenchymal stromal cells for osteochondral tissue regeneration in the rabbit knee joint. *Biofabrication* **2016**, *8*, 14102. [CrossRef] [PubMed]

99. Liu, X.; Liu, S.; Liu, S.; Cui, W. Evaluation of oriented electrospun fibers for periosteal flap regeneration in biomimetic triphasic osteochondral implant. *J. Biomed. Mater. Res. B. Appl. Biomater.* **2014**, *102*, 1407–1414. [CrossRef]

100. Park, J.Y.; Choi, J.-C.; Shim, J.-H.; Lee, J.-S.; Park, H.; Kim, S.W.; Doh, J.; Cho, D.-W. A comparative study on collagen type I and hyaluronic acid dependent cell behavior for osteochondral tissue bioprinting. *Biofabrication* **2014**, *6*, 35004. [CrossRef]

101. Mancini, I.A.D.; Vindas Bolaños, R.A.; Brommer, H.; Castilho, M.; Ribeiro, A.; van Loon, J.P.A.M.; Mensinga, A.; van Rijen, M.H.P.; Malda, J.; van Weeren, R. Fixation of Hydrogel Constructs for Cartilage Repair in the Equine Model: A Challenging Issue. *Tissue Eng. Part C Methods* **2017**, *23*, 804–814. [CrossRef]

102. Liu, X.; Wei, Y.; Xuan, C.; Liu, L.; Lai, C.; Chai, M.; Zhang, Z.; Wang, L.; Shi, X. A Biomimetic Biphasic Osteochondral Scaffold with Layer-Specific Release of Stem Cell Differentiation Inducers for the Reconstruction of Osteochondral Defects. *Adv. Healthc. Mater.* **2020**, *9*, 2000076. [CrossRef] [PubMed]

103. Gong, L.; Li, J.; Zhang, J.; Pan, Z.; Liu, Y.; Zhou, F.; Hong, Y.; Hu, Y.; Gu, Y.; Ouyang, H.; et al. An interleukin-4-loaded bi-layer 3D printed scaffold promotes osteochondral regeneration. *Acta Biomater.* **2020**, *117*, 246–260. [CrossRef] [PubMed]

104. Kosik-Kozioł, A.; Heljak, M.; Święszkowski, W. Mechanical properties of hybrid triphasic scaffolds for osteochondral tissue engineering. *Mater. Lett.* **2020**, *261*, 126893. [CrossRef]

105. Diloksumpan, P.; de Ruijter, M.; Castilho, M.; Gbureck, U.; Vermonden, T.; van Weeren, P.R.; Malda, J.; Levato, R. Combining multi-scale 3D printing technologies to engineer reinforced hydrogel-ceramic interfaces. *Biofabrication* **2020**, *12*, 025014. [CrossRef] [PubMed]

106. Jeon, J.E.; Vaquette, C.; Theodoropoulos, C.; Klein, T.J.; Hutmacher, D.W. Multiphasic construct studied in an ectopic osteochondral defect model. *J. R. Soc. Interface* **2014**, *11*, 20140184. [CrossRef] [PubMed]

107. Zhu, M.; He, X.; Xin, C.; Zhu, Y.; Liu, Z. 3D printing of an integrated triphasic MBG-alginate scaffold with enhanced interface bonding for hard tissue applications. *J. Mater. Sci. Mater. Med.* **2020**, *31*, 113. [CrossRef] [PubMed]

108. Zhang, H.; Huang, H.; Hao, G.; Zhang, Y.; Ding, H.; Fan, Z.; Sun, L. 3D Printing Hydrogel Scaffolds with Nanohydroxyapatite Gradient to Effectively Repair Osteochondral Defects in Rats. *Adv. Funct. Mater.* **2021**, *31*, 2006697. [CrossRef]

109. Kilian, D.; Ahlfeld, T.; Akkineni, A.R.; Bernhardt, A.; Gelinsky, M.; Lode, A. 3D Bioprinting of osteochondral tissue substitutes–in vitro-chondrogenesis in multi-layered mineralized constructs. *Sci. Rep.* **2020**, *10*, 8277. [CrossRef]

110. Critchley, S.; Sheehy, E.J.; Cunniffe, G.; Diaz-Payno, P.; Carroll, S.F.; Jeon, O.; Alsberg, E.; Brama, P.A.J.; Kelly, D.J. 3D printing of fibre-reinforced cartilaginous templates for the regeneration of osteochondral defects. *Acta Biomater.* **2020**, *113*, 130–143. [CrossRef] [PubMed]

111. Pepelanova, I.; Kruppa, K.; Scheper, T.; Lavrentieva, A. Gelatin-Methacryloyl (GelMA) Hydrogels with Defined Degree of Functionalization as a Versatile Toolkit for 3D Cell Culture and Extrusion Bioprinting. *Bioengineering* **2018**, *5*, 55. [CrossRef] [PubMed]

112. Dienes, J.; Browne, S.; Farjun, B.; Amaral Passipieri, J.; Mintz, E.L.; Killian, G.; Healy, K.E.; Christ, G.J. Semisynthetic Hyaluronic Acid-Based Hydrogel Promotes Recovery of the Injured Tibialis Anterior Skeletal Muscle Form and Function. *ACS Biomater. Sci. Eng.* **2021**, *7*, 1587–1599. [CrossRef]

113. Gao, F.; Xu, Z.; Liang, Q.; Liu, B.; Li, H.; Wu, Y.; Zhang, Y.; Lin, Z.; Wu, M.; Ruan, C.; et al. Direct 3D Printing of High Strength Biohybrid Gradient Hydrogel Scaffolds for Efficient Repair of Osteochondral Defect. *Adv. Funct. Mater.* **2018**, *28*, 1706644. [CrossRef]

114. Nooeaid, P.; Salih, V.; Beier, J.P.; Boccaccini, A.R. Osteochondral tissue engineering: Scaffolds, stem cells and applications. *J. Cell. Mol. Med.* **2012**, *16*, 2247–2270. [CrossRef] [PubMed]

115. Reddy, M.S.; Ponnamma, D.; Choudhary, R.; Sadasivuni, K.K. A Comparative Review of Natural and Synthetic Biopolymer Composite Scaffolds. *Polymers* **2021**, *13*, 1105. [CrossRef] [PubMed]

116. Doyle, S.; Henry, L.; McGennisken, E.; Onofrillo, C.; Bella, C.; Duchi, S.; O'Connell, C.; Pirogova, E. Characterization of Polycaprolactone Nanohydroxyapatite Composites with Tunable Degradability Suitable for Indirect Printing. *Polymers* **2021**, *13*, 295. [CrossRef] [PubMed]

117. Li, L.; Li, J.; Guo, J.; Zhang, H.; Zhang, X.; Yin, C.; Wang, L.; Zhu, Y.; Yao, Q. 3D Molecularly Functionalized Cell-Free Biomimetic Scaffolds for Osteochondral Regeneration. *Adv. Funct. Mater.* **2019**, *29*, 1807356. [CrossRef]

118. Malikmammadov, E.; Tanir, T.E.; Kiziltay, A.; Hasirci, V.; Hasirci, N. PCL and PCL-based materials in biomedical applications. *J. Biomater. Sci. Polym. Ed.* **2018**, *29*, 863–893. [CrossRef]

119. Thunsiri, K.; Pitjamit, S.; Pothacharoen, P.; Pruksakorn, D.; Nakkiew, W.; Wattanutchariya, W. The 3D-Printed Bilayer's Bioactive-Biomaterials Scaffold for Full-Thickness Articular Cartilage Defects Treatment. *Materials* **2020**, *13*, 3417. [CrossRef] [PubMed]

120. Di Luca, A.; Longoni, A.; Criscenti, G.; Lorenzo-Moldero, I.; Klein-Gunnewiek, M.; Vancso, J.; van Blitterswijk, C.; Mota, C.; Moroni, L. Surface energy and stiffness discrete gradients in additive manufactured scaffolds for osteochondral regeneration. *Biofabrication* **2016**, *8*, 15014. [CrossRef] [PubMed]

121. Zhang, T.; Zhang, H.; Zhang, L.; Jia, S.; Liu, J.; Xiong, Z.; Sun, W. Biomimetic design and fabrication of multilayered osteochondral scaffolds by low-temperature deposition manufacturing and thermal-induced phase-separation techniques. *Biofabrication* **2017**, *9*, 25021. [CrossRef] [PubMed]

122. Natarajan, A.B.M.; Sivadas, V.P.; Nair, P.D.P. 3D-printed biphasic scaffolds for the simultaneous regeneration of osteochondral tissues. *Biomed. Mater.* **2021**, *16*, 054102. [CrossRef] [PubMed]

123. Wu, X.; Lian, Q.; Li, D.; Jin, Z. Biphasic osteochondral scaffold fabrication using multi-material mask projection stereolithography. *Rapid Prototyp. J.* **2019**, *25*, 277–288. [CrossRef]

124. Zhang, W.; Lian, Q.; Li, D.; Wang, K.; Hao, D.; Bian, W.; He, J.; Jin, Z. Cartilage repair and subchondral bone migration using 3D printing osteochondral composites: A one-year-period study in rabbit trochlea. *Biomed Res. Int.* **2014**, *2014*, 746138. [CrossRef] [PubMed]

125. Zhu, S.; Chen, P.; Chen, Y.; Li, M.; Chen, C.; Lu, H. 3D-Printed Extracellular Matrix/Polyethylene Glycol Diacrylate Hydrogel Incorporating the Anti-inflammatory Phytomolecule Honokiol for Regeneration of Osteochondral Defects. *Am. J. Sports Med.* **2020**, *48*, 2808–2818. [CrossRef]

126. Zhu, J. Bioactive modification of poly(ethylene glycol) hydrogels for tissue engineering. *Biomaterials* **2010**, *31*, 4639–4656. [CrossRef] [PubMed]

127. Lin, C.-C.; Anseth, K.S. PEG Hydrogels for the Controlled Release of Biomolecules in Regenerative Medicine. *Pharm. Res.* **2009**, *26*, 631–643. [CrossRef] [PubMed]

128. Wang, M.; Guo, L.; Sun, H. Manufacture of Biomaterials. In *Encyclopedia of Biomedical Engineering*; Narayan, R., Ed.; Elsevier: Oxford, UK, 2019; pp. 116–134. ISBN 978-0-12-805144-3.

129. Yousefi, A.-M.; Hoque, M.E.; Prasad, R.G.; Uth, N. Current strategies in multiphasic scaffold design for osteochondral tissue engineering: A review. *J. Biomed. Mater. Res. A* **2015**, *103*, 2460–2481. [CrossRef]

130. Hsieh, Y.-H.; Hsieh, M.-F.; Fang, C.-H.; Jiang, C.-P.; Lin, B.; Lee, H.-M. Osteochondral Regeneration Induced by TGF-beta Loaded Photo Cross-Linked Hyaluronic Acid Hydrogel Infiltrated in Fused Deposition-Manufactured Composite Scaffold of Hydroxyapatite and Poly (Ethylene Glycol)-Block-Poly(epsilon-Caprolactone). *Polymers* **2017**, *9*, 182. [CrossRef] [PubMed]

131. Moses, J.C.; Saha, T.; Mandal, B.B. Chondroprotective and osteogenic effects of silk-based bioinks in developing 3D bioprinted osteochondral interface. *Bioprinting* **2020**, *17*, e00067. [CrossRef]

132. Bellucci, D.; Sola, A.; Cannillo, V. Hydroxyapatite and tricalcium phosphate composites with bioactive glass as second phase: State of the art and current applications. *J. Biomed. Mater. Res. Part A* **2016**, *104*, 1030–1056. [CrossRef] [PubMed]

133. Baino, F.; Novajra, G.; Vitale-Brovarone, C. Bioceramics and Scaffolds: A Winning Combination for Tissue Engineering. *Front. Bioeng. Biotechnol.* **2015**, *3*, 202. [CrossRef] [PubMed]

134. Deng, C.; Chang, J.; Wu, C. Bioactive scaffolds for osteochondral regeneration. *J. Orthop. Transl.* **2019**, *17*, 15–25. [CrossRef]

135. Nyberg, E.; Rindone, A.; Dorafshar, A.; Grayson, W.L. Comparison of 3D-Printed Poly-*ε*-Caprolactone Scaffolds Functionalized with Tricalcium Phosphate, Hydroxyapatite, Bio-Oss, or Decellularized Bone Matrix. *Tissue Eng. Part A* **2017**, *23*, 503–514. [CrossRef] [PubMed]

136. Zhu, W.; Ma, X.; Gou, M.; Mei, D.; Zhang, K.; Chen, S. 3D printing of functional biomaterials for tissue engineering. *Curr. Opin. Biotechnol.* **2016**, *40*, 103–112. [CrossRef]

137. Adamkiewicz, M.; Rubinsky, B. Cryogenic 3D printing for tissue engineering. *Cryobiology* **2015**, *71*, 518–521. [CrossRef] [PubMed]

138. Zhou, Z.; Buchanan, F.; Mitchell, C.; Dunne, N. Printability of calcium phosphate: Calcium sulfate powders for the application of tissue engineered bone scaffolds using the 3D printing technique. *Mater. Sci. Eng. C* **2014**, *38*, 1–10. [CrossRef]

139. Du, Y.; Liu, H.; Yang, Q.; Wang, S.; Wang, J.; Ma, J.; Noh, I.; Mikos, A.G.; Zhang, S. Selective laser sintering scaffold with hierarchical architecture and gradient composition for osteochondral repair in rabbits. *Biomaterials* **2017**, *137*, 37–48. [CrossRef]

140. Castro, N.J.; Patel, R.; Zhang, L.G. Design of a Novel 3D Printed Bioactive Nanocomposite Scaffold for Improved Osteochondral Regeneration. *Cell. Mol. Bioeng.* **2015**, *8*, 416–432. [CrossRef] [PubMed]

141. Nowicki, M.; Zhu, W.; Sarkar, K.; Rao, R.; Zhang, L.G. 3D printing multiphasic osteochondral tissue constructs with nano to micro features via PCL based bioink. *Bioprinting* **2020**, *17*, e00066. [CrossRef]

142. Lee, J.-Y.; Choi, B.; Wu, B.; Lee, M. Customized biomimetic scaffolds created by indirect three-dimensional printing for tissue engineering. *Biofabrication* **2013**, *5*, 45003. [CrossRef] [PubMed]

143. Li, Z.; Jia, S.; Xiong, Z.; Long, Q.; Yan, S.; Hao, F.; Liu, J.; Yuan, Z. 3D-printed scaffolds with calcified layer for osteochondral tissue engineering. *J. Biosci. Bioeng.* **2018**, *126*, 389–396. [CrossRef]

144. Doyle, S.E.; Duchi, S.; Onofrillo, C.; Quigley, A.; Di Bella, C.; Pirogova, E.; O'Connell, C.D. Printing between the Lines: Intricate Biomaterial Structures Fabricated via Negative Embodied Sacrificial Template 3D (NEST3D) Printing. *Adv. Mater. Technol.* **2021**, *6*, 7. [CrossRef]

145. Jiwoon, L.; Jesse, W.; Sanjay, N.; Sung, Y. Prediction of geometric characteristics in polycaprolactone (PCL) scaffolds produced by extrusion-based additive manufacturing technique for tissue engineering. *Rapid Prototyp. J.* **2019**, *26*, 238–248.

146. Sodupe Ortega, E.; Sanz-Garcia, A.; Pernia-Espinoza, A.; Escobedo-Lucea, C. Efficient Fabrication of Polycaprolactone Scaffolds for Printing Hybrid Tissue-Engineered Constructs. *Materials* **2019**, *12*, 613. [CrossRef]

147. O'Connell, C.D.; Konate, S.; Onofrillo, C.; Kapsa, R.; Baker, C.; Duchi, S.; Eekel, T.; Yue, Z.; Beirne, S.; Barnsley, G.; et al. Free-form co-axial bioprinting of a gelatin methacryloyl bio-ink by direct in situ photo-crosslinking during extrusion. *Bioprinting* **2020**, *19*, e00087. [CrossRef]

148. O'Connell, C.; Ren, J.; Pope, L.; Li, Y.; Mohandas, A.; Blanchard, R.; Duchi, S.; Onofrillo, C. Characterizing Bioinks for Extrusion Bioprinting: Printability and Rheology. *Methods Mol. Biol.* **2020**, *2140*, 111–133.

149. Leong, K.F.; Cheah, C.M.; Chua, C.K. Solid freeform fabrication of three-dimensional scaffolds for engineering replacement tissues and organs. *Biomaterials* **2003**, *24*, 2363–2378. [CrossRef]

150. Mikos, A.G.; Sarakinos, G.; Lyman, M.D.; Ingber, D.E.; Vacanti, J.P.; Langer, R. Prevascularization of porous biodegradable polymers. *Biotechnol. Bioeng.* **1993**, *42*, 716–723. [CrossRef] [PubMed]

151. Gupte, M.J.; Swanson, W.B.; Hu, J.; Jin, X.; Ma, H.; Zhang, Z.; Liu, Z.; Feng, K.; Feng, G.; Xiao, G.; et al. Pore size directs bone marrow stromal cell fate and tissue regeneration in nanofibrous macroporous scaffolds by mediating vascularization. *Acta Biomater.* **2018**, *82*, 1–11. [CrossRef]

152. Karageorgiou, V.; Kaplan, D. Porosity of 3D biomaterial scaffolds and osteogenesis. *Biomaterials* **2005**, *26*, 5474–5491. [CrossRef]

153. Li, G.; Wang, L.; Pan, W.; Yang, F.; Jiang, W.; Wu, X.; Kong, X.; Dai, K.; Hao, Y. In vitro and in vivo study of additive manufactured porous Ti6Al4V scaffolds for repairing bone defects. *Sci. Rep.* **2016**, *6*, 34072. [CrossRef] [PubMed]

154. Ginestra, P.; Pandini, S.; Ceretti, E. Hybrid multi-layered scaffolds produced via grain extrusion and electrospinning for 3D cell culture tests. *Rapid Prototyp. J.* **2020**, *26*, 593–602. [CrossRef]

155. Deng, C.; Zhu, H.; Li, J.; Feng, C.; Yao, Q.; Wang, L.; Chang, J.; Wu, C. Bioactive Scaffolds for Regeneration of Cartilage and Subchondral Bone Interface. *Theranostics* **2018**, *8*, 1940–1955. [CrossRef]

156. Chen, L.; Deng, C.; Li, J.; Yao, Q.; Chang, J.; Wang, L.; Wu, C. 3D printing of a lithium-calcium-silicate crystal bioscaffold with dual bioactivities for osteochondral interface reconstruction. *Biomaterials* **2019**, *196*, 138–150. [CrossRef] [PubMed]

157. Dang, W.; Wang, X.; Li, J.; Deng, C.; Liu, Y.; Yao, Q.; Wang, L.; Chang, J.; Wu, C. 3D printing of Mo-containing scaffolds with activated anabolic responses and bi-lineage bioactivities. *Theranostics* **2018**, *8*, 4372–4392. [CrossRef] [PubMed]

158. Annabi, N.; Nichol, J.W.; Zhong, X.; Ji, C.; Koshy, S.; Khademhosseini, A.; Dehghani, F. Controlling the porosity and microarchitecture of hydrogels for tissue engineering. *Tissue Eng. Part B Rev.* **2010**, *16*, 371–383. [CrossRef] [PubMed]

159. de Lima, C.S.A.; Balogh, T.S.; Varca, J.P.R.O.; Varca, G.H.C.; Lugão, A.B.; Camacho-Cruz, L.A.; Bucio, E.; Kadlubowski, S.S. An Updated Review of Macro, Micro, and Nanostructured Hydrogels for Biomedical and Pharmaceutical Applications. *Pharmaceutics* **2020**, *12*, 970. [CrossRef]

160. Dalton, P.D. Melt electrowriting with additive manufacturing principles. *Curr. Opin. Biomed. Eng.* **2017**, *2*, 49–57. [CrossRef]

161. Yoon, Y.I.; Park, K.E.; Lee, S.J.; Park, W.H. Fabrication of Microfibrous and Nano-/Microfibrous Scaffolds: Melt and Hybrid Electrospinning and Surface Modification of Poly(L-lactic acid) with Plasticizer. *Biomed Res. Int.* **2013**, *2013*, 309010–309048. [CrossRef] [PubMed]

162. Brown, T.D.; Dalton, P.D.; Hutmacher, D.W. Direct Writing By Way of Melt Electrospinning. *Adv. Mater.* **2011**, *23*, 5651–5657. [CrossRef]

163. Kade, J.C.; Dalton, P.D. Polymers for Melt Electrowriting. *Adv. Healthc. Mater.* **2021**, *10*, 2001232. [CrossRef] [PubMed]

164. O'Connell, C.D.; Bridges, O.; Everett, C.; Antill-O'Brien, N.; Onofrillo, C.; Di Bella, C. Electrostatic Distortion of Melt-Electrowritten Patterns by 3D Objects: Quantification, Modeling, and Toolpath Correction. *Adv. Mater. Technol.* **2021**, *6*, 2100345. [CrossRef]

165. Hejazi, F.; Bagheri-Khoulenjani, S.; Olov, N.; Zeini, D.; Solouk, A.; Mirzadeh, H. Fabrication of nanocomposite/nanofibrous functionally graded biomimetic scaffolds for osteochondral tissue regeneration. *J. Biomed. Mater. Res. Part A* **2021**, *109*, 1657–1669. [CrossRef]

166. Ho, S.T.B.; Hutmacher, D.W.; Ekaputra, A.K.; Hitendra, D.; Hui, J.H. The evaluation of a biphasic osteochondral implant coupled with an electrospun membrane in a large animal model. *Tissue Eng. Part A* **2010**, *16*, 1123–1141. [CrossRef]

167. Agarwal, S.; Greiner, A. On the way to clean and safe electrospinning—Green electrospinning: Emulsion and suspension electrospinning. *Polym. Adv. Technol.* **2011**, *22*, 372–378. [CrossRef]

168. Wortmann, M.; Frese, N.; Sabantina, L.; Petkau, R.; Kinzel, F.; Gölzhäuser, A.; Moritzer, E.; Hüsgen, B.; Ehrmann, A. New Polymers for Needleless Electrospinning from Low-Toxic Solvents. *Nanomaterials* **2019**, *9*, 52. [CrossRef]

169. Saidy, N.T.; Shabab, T.; Bas, O.; Rojas-González, D.M.; Menne, M.; Henry, T.; Hutmacher, D.W.; Mela, P.; De-Juan-Pardo, E.M. Melt Electrowriting of Complex 3D Anatomically Relevant Scaffolds. *Front. Bioeng. Biotechnol.* **2020**, *8*, 793. [CrossRef]

170. Brown, T.D.; Dalton, P.D.; Hutmacher, D.W. Melt electrospinning today: An opportune time for an emerging polymer process. *Prog. Polym. Sci.* **2016**, *56*, 116–166. [CrossRef]

171. Wunner, F.M.; Wille, M.-L.; Noonan, T.G.; Bas, O.; Dalton, P.D.; De-Juan-Pardo, E.M.; Hutmacher, D.W. Melt Electrospinning Writing of Highly Ordered Large Volume Scaffold Architectures. *Adv. Mater.* **2018**, *30*, 1706570. [CrossRef]

172. Cui, Z.; Wright, L.D.; Guzzo, R.; Freeman, J.W.; Drissi, H.; Nair, L.S. Poly(d-lactide)/poly(caprolactone) nanofiber-thermogelling chitosan gel composite scaffolds for osteochondral tissue regeneration in a rat model. *J. Bioact. Compat. Polym.* **2013**, *28*, 115–125. [CrossRef]

173. Stansbury, J.W.; Idacavage, M.J. 3D printing with polymers: Challenges among expanding options and opportunities. *Dent. Mater.* **2016**, *32*, 54–64. [CrossRef] [PubMed]

174. Derakhshanfar, S.; Mbeleck, R.; Xu, K.; Zhang, X.; Zhong, W.; Xing, M. 3D bioprinting for biomedical devices and tissue engineering: A review of recent trends and advances. *Bioact. Mater.* **2018**, *3*, 144–156. [CrossRef]

175. Wang, Z.; Abdulla, R.; Parker, B.; Samanipour, R.; Ghosh, S.; Kim, K. A simple and high-resolution stereolithography-based 3D bioprinting system using visible light crosslinkable bioinks. *Biofabrication* **2015**, *7*, 045009. [CrossRef] [PubMed]

176. Manapat, J.Z.; Chen, Q.; Ye, P.; Advincula, R.C. 3D Printing of Polymer Nanocomposites via Stereolithography. *Macromol. Mater. Eng.* **2017**, *302*, 1600553. [CrossRef]

177. Li, F.; Macdonald, N.P.; Guijt, R.M.; Breadmore, M.C. Increasing the functionalities of 3D printed microchemical devices by single material, multimaterial, and print-pause-print 3D printing. *Lab Chip* **2019**, *19*, 35–49. [CrossRef]

178. Fiedor, P.; Ortyl, J. A New Approach to Micromachining: High-Precision and Innovative Additive Manufacturing Solutions Based on Photopolymerization Technology. *Materials* **2020**, *13*, 2951. [CrossRef]

179. Kumar, H.; Sakthivel, K.; Mohamed, M.G.A.; Boras, E.; Shin, S.R.; Kim, K. Designing Gelatin Methacryloyl (GelMA)-Based Bioinks for Visible Light Stereolithographic 3D Biofabrication. *Macromol. Biosci.* **2021**, *21*, 2000317. [CrossRef] [PubMed]

180. Schoonraad, S.A.; Fischenich, K.M.; Eckstein, K.N.; Crespo-Cuevas, V.; Savard, L.M.; Muralidharan, A.; Tomaschke, A.A.; Uzcategui, A.C.; Randolph, M.A.; McLeod, R.R.; et al. Biomimetic and mechanically supportive 3D printed scaffolds for cartilage and osteochondral tissue engineering using photopolymers and digital light processing. *Biofabrication* **2021**, *13*, 44106. [CrossRef]

181. Bian, W.; Li, D.; Lian, Q.; Li, X.; Zhang, W.; Wang, K.; Jin, Z. Fabrication of a bio-inspired beta-Tricalcium phosphate/collagen scaffold based on ceramic stereolithography and gel casting for osteochondral tissue engineering. *Rapid Prototyp. J.* **2012**, *18*, 68–80. [CrossRef]

182. Castro, N.J.; O'Brien, J.; Zhang, L.G. Integrating biologically inspired nanomaterials and table-top stereolithography for 3D printed biomimetic osteochondral scaffolds. *Nanoscale* **2015**, *7*, 14010–14022. [CrossRef] [PubMed]

183. Suo, H.; Chen, Y.; Liu, J.; Wang, L.; Xu, M. 3D printing of biphasic osteochondral scaffold with sintered hydroxyapatite and polycaprolactone. *J. Mater. Sci.* **2021**, *56*, 16623–16633. [CrossRef]

184. Qiao, Z.; Lian, M.; Han, Y.; Sun, B.; Zhang, X.; Jiang, W.; Li, H.; Hao, Y.; Dai, K. Bioinspired stratified electrowritten fiber-reinforced hydrogel constructs with layer-specific induction capacity for functional osteochondral regeneration. *Biomaterials* **2021**, *266*, 120385. [CrossRef]

185. Hernandez, J.L.; Park, J.; Yao, S.; Blakney, A.K.; Nguyen, H.V.; Katz, B.H.; Jensen, J.T.; Woodrow, K.A. Effect of tissue microenvironment on fibrous capsule formation to biomaterial-coated implants. *Biomaterials* **2021**, *273*, 120806. [CrossRef] [PubMed]

186. Carnicer-Lombarte, A.; Chen, S.-T.; Malliaras, G.G.; Barone, D.G. Foreign Body Reaction to Implanted Biomaterials and Its Impact in Nerve Neuroprosthetics. *Front. Bioeng. Biotechnol.* **2021**, *9*, 271. [CrossRef] [PubMed]

187. Klopfleisch, R.; Jung, F. The pathology of the foreign body reaction against biomaterials. *J. Biomed. Mater. Res. Part A* **2017**, *105*, 927–940. [CrossRef] [PubMed]

188. Hilborn, J.; Bjursten, L.M. A new and evolving paradigm for biocompatibility. *J. Tissue Eng. Regen. Med.* **2007**, *1*, 110–119. [CrossRef] [PubMed]

189. Jani, M.M.; Parker, R.D. Internal fixation devices for the treatment of unstable osteochondritis dissecans and chondral lesions. *Oper. Tech. Sports Med.* **2004**, *12*, 170–175. [CrossRef]

190. Wei, P.; Xu, Y.; Zhang, H.; Wang, L. Continued sustained insulin-releasing PLGA nanoparticles modified 3D-Printed PCL composite scaffolds for osteochondral repair. *Chem. Eng. J.* **2021**, *422*, 130051. [CrossRef]

191. Hu, X.; Man, Y.; Li, W.; Li, L.; Xu, J.; Parungao, R.; Wang, Y.; Zheng, S.; Nie, Y.; Liu, T.; et al. 3D Bio-Printing of CS/Gel/HA/Gr Hybrid Osteochondral Scaffolds. *Polymers* **2019**, *11*, 1601. [CrossRef]

192. Wang, C.; Yue, H.; Huang, W.; Lin, X.; Xie, X.; He, Z.; He, X.; Liu, S.; Bai, L.; Lu, B.; et al. Cryogenic 3D printing of heterogeneous scaffolds with gradient mechanical strengths and spatial delivery of osteogenic peptide/TGF-β1 for osteochondral tissue regeneration. *Biofabrication* **2020**, *12*, 25030. [CrossRef]

193. Bittner, S.M.; Smith, B.T.; Diaz-Gomez, L.; Hudgins, C.D.; Melchiorri, A.J.; Scott, D.W.; Fisher, J.P.; Mikos, A.G. Fabrication and mechanical characterization of 3D printed vertical uniform and gradient scaffolds for bone and osteochondral tissue engineering. *Acta Biomater.* **2019**, *90*, 37–48. [CrossRef]

194. Gonzalez-Fernandez, T.; Rathan, S.; Hobbs, C.; Pitacco, P.; Freeman, F.E.; Cunniffe, G.M.; Dunne, N.J.; McCarthy, H.O.; Nicolosi, V.; O'Brien, F.J.; et al. Pore-forming bioinks to enable spatio-temporally defined gene delivery in bioprinted tissues. *J. Control. Release* **2019**, *301*, 13–27. [CrossRef] [PubMed]

195. Gao, G.; Yonezawa, T.; Hubbell, K.; Dai, G.; Cui, X. Inkjet-bioprinted acrylated peptides and PEG hydrogel with human mesenchymal stem cells promote robust bone and cartilage formation with minimal printhead clogging. *Biotechnol. J.* **2015**, *10*, 1568–1577. [CrossRef]

196. Deng, C.; Lin, R.; Zhang, M.; Qin, C.; Yao, Q.; Wang, L.; Chang, J.; Wu, C. Micro/Nanometer-Structured Scaffolds for Regeneration of Both Cartilage and Subchondral Bone. *Adv. Funct. Mater.* **2019**, *29*, 1806068. [CrossRef]

197. Ahlfeld, T.; Doberenz, F.; Kilian, D.; Vater, C.; Korn, P.; Lauer, G.; Lode, A.; Gelinsky, M. Bioprinting of mineralized constructs utilizing multichannel plotting of a self-setting calcium phosphate cement and a cell-laden bioink. *Biofabrication* **2018**, *10*, 45002. [CrossRef] [PubMed]

198. Ko, J.-Y.; Kim, K.-I.; Park, S.; Im, G.-I. In vitro chondrogenesis and in vivo repair of osteochondral defect with human induced pluripotent stem cells. *Biomaterials* **2014**, *35*, 3571–3581. [CrossRef] [PubMed]

199. Castro-Viñuelas, R.; Sanjurjo-Rodríguez, C.; Piñeiro-Ramil, M.; Hermida-Gómez, T.; Fuentes-Boquete, I.M.; de Toro-Santos, F.J.; Blanco-García, F.J.; Díaz-Prado, S.M. Induced pluripotent stem cells for cartilage repair: Current status and future perspectives. *Eur. Cell. Mater.* **2018**, *36*, 96–109. [CrossRef]

200. Diekman, B.O.; Christoforou, N.; Willard, V.P.; Sun, H.; Sanchez-Adams, J.; Leong, K.W.; Guilak, F. Cartilage tissue engineering using differentiated and purified induced pluripotent stem cells. *Proc. Natl. Acad. Sci. USA* **2012**, *109*, 19172–19177. [CrossRef]

201. Jha, B.S.; Farnoodian, M.; Bharti, K. Regulatory considerations for developing a phase I investigational new drug application for autologous induced pluripotent stem cells-based therapy product. *Stem Cells Transl. Med.* **2021**, *10*, 198–208. [CrossRef] [PubMed]

202. Charlier, E.; Deroyer, C.; Ciregia, F.; Malaise, O.; Neuville, S.; Plener, Z.; Malaise, M.; de Seny, D. Chondrocyte dedifferentiation and osteoarthritis (OA). *Biochem. Pharmacol.* **2019**, *165*, 49–65. [CrossRef]

203. Yao, Y.; Wang, C. Dedifferentiation: Inspiration for devising engineering strategies for regenerative medicine. *NPJ Regen. Med.* **2020**, *5*, 14. [CrossRef] [PubMed]

204. Vis, M.A.M.; Ito, K.; Hofmann, S. Impact of Culture Medium on Cellular Interactions in in vitro Co-culture Systems. *Front. Bioeng. Biotechnol.* **2020**, *8*, 911. [CrossRef] [PubMed]

205. Zhao, H.; Wu, J.; Zhu, J.; Xiao, Z.; He, C.; Shi, H.; Li, X.; Yang, S.; Xiao, J. Research Advances in Tissue Engineering Materials for Sustained Release of Growth Factors. *Biomed Res. Int.* **2015**, *2015*, 808202. [CrossRef]

206. Ren, X.; Zhao, M.; Lash, B.; Martino, M.M.; Julier, Z. Growth Factor Engineering Strategies for Regenerative Medicine Applications. *Front. Bioeng. Biotechnol.* **2020**, *7*, 469. [CrossRef]

207. Spiller, K.L.; Liu, Y.; Holloway, J.L.; Maher, S.A.; Cao, Y.; Liu, W.; Zhou, G.; Lowman, A.M. A novel method for the direct fabrication of growth factor-loaded microspheres within porous nondegradable hydrogels: Controlled release for cartilage tissue engineering. *J. Control. Release* **2012**, *157*, 39–45. [CrossRef]

208. Kim, J.; Lin, B.; Kim, S.; Choi, B.; Evseenko, D.; Lee, M. TGF-β1 conjugated chitosan collagen hydrogels induce chondrogenic differentiation of human synovium-derived stem cells. *J. Biol. Eng.* **2015**, *9*, 1. [CrossRef]

209. Holland, T.A.; Tabata, Y.; Mikos, A.G. Dual growth factor delivery from degradable oligo(poly(ethylene glycol) fumarate) hydrogel scaffolds for cartilage tissue engineering. *J. Control. Release* **2005**, *101*, 111–125. [CrossRef]

210. Blaney Davidson, E.N.; Vitters, E.L.; van Lent, P.L.E.M.; van de Loo, F.A.J.; van den Berg, W.B.; van der Kraan, P.M. Elevated extracellular matrix production and degradation upon bone morphogenetic protein-2 (BMP-2) stimulation point toward a role for BMP-2 in cartilage repair and remodeling. *Arthritis Res. Ther.* **2007**, *9*, R102. [CrossRef]

211. Knippenberg, M.; Helder, M.N.; Zandieh Doulabi, B.; Wuisman, P.I.J.; Klein-Nulend, J. Osteogenesis versus chondrogenesis by BMP-2 and BMP-7 in adipose stem cells. *Biochem. Biophys. Res. Commun.* **2006**, *342*, 902–908. [CrossRef] [PubMed]

212. Crecente-Campo, J.; Borrajo, E.; Vidal, A.; Garcia-Fuentes, M. New scaffolds encapsulating TGF-β3/BMP-7 combinations driving strong chondrogenic differentiation. *Eur. J. Pharm. Biopharm.* **2017**, *114*, 69–78. [CrossRef] [PubMed]

213. Kaul, G.; Cucchiarini, M.; Arntzen, D.; Zurakowski, D.; Menger, M.D.; Kohn, D.; Trippel, S.B.; Madry, H. Local stimulation of articular cartilage repair by transplantation of encapsulated chondrocytes overexpressing human fibroblast growth factor 2 (FGF-2) in vivo. *J. Gene Med.* **2006**, *8*, 100–111. [CrossRef]

214. Orth, P.; Kaul, G.; Cucchiarini, M.; Zurakowski, D.; Menger, M.D.; Kohn, D.; Madry, H. Transplanted articular chondrocytes co-overexpressing IGF-I and FGF-2 stimulate cartilage repair in vivo. *Knee Surg. Sports Traumatol. Arthrosc.* **2011**, *19*, 2119–2130. [CrossRef] [PubMed]

215. Lee, K.; Silva, E.A.; Mooney, D.J. Growth factor delivery-based tissue engineering: General approaches and a review of recent developments. *J. R. Soc. Interface* **2011**, *8*, 153–170. [CrossRef]

216. Kieswetter, K.; Schwartz, Z.; Alderete, M.; Dean, D.D.; Boyan, B.D. Platelet derived growth factor stimulates chondrocyte proliferation but prevents endochondral maturation. *Endocrine* **1997**, *6*, 257–264. [CrossRef]

217. Maehara, H.; Sotome, S.; Yoshii, T.; Torigoe, I.; Kawasaki, Y.; Sugata, Y.; Yuasa, M.; Hirano, M.; Mochizuki, N.; Kikuchi, M.; et al. Repair of large osteochondral defects in rabbits using porous hydroxyapatite/collagen (HAp/Col) and fibroblast growth factor-2 (FGF-2). *J. Orthop. Res.* **2010**, *28*, 677–686. [CrossRef]

218. Lu, S.; Lam, J.; Trachtenberg, J.E.; Lee, E.J.; Seyednejad, H.; van den Beucken, J.J.J.P.; Tabata, Y.; Wong, M.E.; Jansen, J.A.; Mikos, A.G.; et al. Dual growth factor delivery from bilayered, biodegradable hydrogel composites for spatially-guided osteochondral tissue repair. *Biomaterials* **2014**, *35*, 8829–8839. [CrossRef]

219. Sun, J.; Lyu, J.; Xing, F.; Chen, R.; Duan, X.; Xiang, Z. A biphasic, demineralized, and Decellularized allograft bone-hydrogel scaffold with a cell-based BMP-7 delivery system for osteochondral defect regeneration. *J. Biomed. Mater. Res. A* **2020**, *108*, 1909–1921. [CrossRef]

220. Wang, Q.; Zhang, H.; Gan, H.; Wang, H.; Li, Q.; Wang, Z. Application of combined porous tantalum scaffolds loaded with bone morphogenetic protein 7 to repair of osteochondral defect in rabbits. *Int. Orthop.* **2018**, *42*, 1437–1448. [CrossRef]

221. Caballero Aguilar, L.M.; Silva, S.M.; Moulton, S.E. Growth factor delivery: Defining the next generation platforms for tissue engineering. *J. Control. Release* **2019**, *306*, 40–58. [CrossRef] [PubMed]

222. Xue, R.; Chung, B.; Tamaddon, M.; Carr, J.; Liu, C.; Cartmell, S.H. Osteochondral tissue coculture: An in vitro and in silico approach. *Biotechnol. Bioeng.* **2019**, *116*, 3112–3123. [CrossRef] [PubMed]

223. Cipriani, F.; Krueger, M.; González, I.; Sierra, L.; Alonso, M.; Kock, L.; Rodríguez-Cabello, J. Cartilage Regeneration in Preannealed Silk Elastin-Like Co-Recombinamers Injectable Hydrogel Embedded with Mature Chondrocytes in an Ex Vivo Culture Platform. *Biomacromolecules* **2018**, *19*, 4333–4347. [CrossRef] [PubMed]

224. Hu, W.; Chen, Y.; Dou, C.; Dong, S. Microenvironment in subchondral bone: Predominant regulator for the treatment of osteoarthritis. *Ann. Rheum. Dis.* **2021**, *80*, 413–422. [CrossRef]

225. O'Connell, C.D.; Zhang, B.; Onofrillo, C.; Duchi, S.; Blanchard, R.; Quigley, A.; Bourke, J.; Gambhir, S.; Kapsa, R.; Di Bella, C.; et al. Tailoring the mechanical properties of gelatin methacryloyl hydrogels through manipulation of the photocrosslinking conditions. *Soft Matter* **2018**, *14*, 2142–2151. [CrossRef]

226. Loh, Q.L.; Choong, C. Three-dimensional scaffolds for tissue engineering applications: Role of porosity and pore size. *Tissue Eng. Part B Rev.* **2013**, *19*, 485–502. [CrossRef]

227. Abbasi, N.; Hamlet, S.; Love, R.M.; Nguyen, N.-T. Porous scaffolds for bone regeneration. *J. Sci. Adv. Mater. Devices* **2020**, *5*, 1–9. [CrossRef]

228. Khader, A.; Arinzeh, T.L. Biodegradable zinc oxide composite scaffolds promote osteochondral differentiation of mesenchymal stem cells. *Biotechnol. Bioeng.* **2020**, *117*, 194–209. [CrossRef] [PubMed]

229. Mancini, I.A.D.; Schmidt, S.; Brommer, H.; Pouran, B.; Schäfer, S.; Tessmar, J.; Mensinga, A.; van Rijen, M.H.P.; Groll, J.; Blunk, T.; et al. A composite hydrogel-3D printed thermoplast osteochondral anchor as example for a zonal approach to cartilage repair: In vivo performance in a long-term equine model. *Biofabrication* **2020**, *12*, 35028. [CrossRef]

230. National Academies of Sciences, Engineering, and Medicine. *Advancing Disease Modeling in Animal-Based Research in Support of Precision Medicine: Proceedings of a Workshop*; The National Academies Press: Washington, DC, USA, 2018; ISBN 978-0-309-47116-9.

231. De Pieri, A.; Korman, B.D.; Jüngel, A.; Wuertz-Kozak, K. Engineering Advanced In Vitro Models of Systemic Sclerosis for Drug Discovery and Development. *Adv. Biol.* **2021**, *5*, 2000168. [CrossRef]

232. Nikolakopoulou, P.; Rauti, R.; Voulgaris, D.; Shlomy, I.; Maoz, B.M.; Herland, A. Recent progress in translational engineered in vitro models of the central nervous system. *Brain* **2020**, *143*, 3181–3213. [CrossRef] [PubMed]

233. Schwab, A.; Buss, A.; Pullig, O.; Ehlicke, F. Ex vivo osteochondral test system with control over cartilage defect depth—A pilot study to investigate the effect of oxygen tension and chondrocyte-based treatments in chondral and full thickness defects in an organ model. *bioRxiv* **2021**, *3*, 100173. [CrossRef]

234. Aisenbrey, E.A.; Tomaschke, A.; Kleinjan, E.; Muralidharan, A.; Pascual-Garrido, C.; McLeod, R.R.; Ferguson, V.L.; Bryant, S.J. A Stereolithography-Based 3D Printed Hybrid Scaffold for In Situ Cartilage Defect Repair. *Macromol. Biosci.* **2018**, *18*, 1700267. [CrossRef] [PubMed]

235. Mouser, V.H.M.; Dautzenberg, N.M.M.; Levato, R.; van Rijen, M.H.P.; Dhert, W.J.A.; Malda, J.; Gawlitta, D. Ex vivo model unravelling cell distribution effect in hydrogels for cartilage repair. *ALTEX* **2018**, *35*, 65–76. [CrossRef]

236. Schmutzer, M.; Aszodi, A. Cell compaction influences the regenerative potential of passaged bovine articular chondrocytes in an ex vivo cartilage defect model. *J. Biosci. Bioeng.* **2017**, *123*, 512–522. [CrossRef]

237. de Vries-van Melle, M.L.; Mandl, E.W.; Kops, N.; Koevoet, W.J.L.M.; Verhaar, J.A.N.; van Osch, G.J.V.M. An osteochondral culture model to study mechanisms involved in articular cartilage repair. *Tissue Eng. Part C Methods* **2012**, *18*, 45–53. [CrossRef]

238. Duchi, S.; Doyle, S.; Eekel, T.; O'Connell, C.D.; Augustine, C.; Choong, P.; Onofrillo, C.; Di Bella, C. Protocols for Culturing and Imaging a Human Ex Vivo Osteochondral Model for Cartilage Biomanufacturing Applications. *Materials* **2019**, *12*, 640. [CrossRef]

239. Malda, J.; Benders, K.E.M.; Klein, T.J.; de Grauw, J.C.; Kik, M.J.L.; Hutmacher, D.W.; Saris, D.B.F.; van Weeren, P.R.; Dhert, W.J.A. Comparative study of depth-dependent characteristics of equine and human osteochondral tissue from the medial and lateral femoral condyles. *Osteoarthr. Cartil.* **2012**, *20*, 1147–1151. [CrossRef] [PubMed]
240. Madry, H.; Ochi, M.; Cucchiarini, M.; Pape, D.; Seil, R. Large animal models in experimental knee sports surgery: Focus on clinical translation. *J. Exp. Orthop.* **2015**, *2*, 9. [CrossRef]
241. Chu, C.R.; Szczodry, M.; Bruno, S. Animal models for cartilage regeneration and repair. *Tissue Eng. Part B Rev.* **2010**, *16*, 105–115. [CrossRef]
242. McGowan, K.B.; Stiegman, G. Regulatory Challenges for Cartilage Repair Technologies. *Cartilage* **2012**, *4*, 4–11. [CrossRef] [PubMed]
243. Hsieh, Y.-H.; Shen, B.-Y.; Wang, Y.-H.; Lin, B.; Lee, H.-M.; Hsieh, M.-F. Healing of Osteochondral Defects Implanted with Biomimetic Scaffolds of Poly(ε-Caprolactone)/Hydroxyapatite and Glycidyl-Methacrylate-Modified Hyaluronic Acid in a Minipig. *Int. J. Mol. Sci.* **2018**, *19*, 1125. [CrossRef] [PubMed]
244. Abdollahi, S.; Davis, A.; Miller, J.H.; Feinberg, A.W. Expert-guided optimization for 3D printing of soft and liquid materials. *PLoS ONE* **2018**, *13*, e0194890. [CrossRef] [PubMed]
245. Bawolin, N.K.; Zhang, W.J.; Chen, X.B. A Brief Review of the Modelling of the Time Dependent Mechanical Properties of Tissue Engineering Scaffolds. *J. Biomimetics Biomater. Tissue Eng.* **2010**, *6*, 19–33. [CrossRef]
246. Andani, M.T.; Shayesteh Moghaddam, N.; Haberland, C.; Dean, D.; Miller, M.J.; Elahinia, M. Metals for bone implants. Part 1. Powder metallurgy and implant rendering. *Acta Biomater.* **2014**, *10*, 4058–4070. [CrossRef]
247. Raut, H.K.; Das, R.; Liu, Z.; Liu, X.; Ramakrishna, S. Biocompatibility of Biomaterials for Tissue Regeneration or Replacement. *Biotechnol. J.* **2020**, *15*, 2000160. [CrossRef]
248. Zhou, X.; Esworthy, T.; Lee, S.-J.; Miao, S.; Cui, H.; Plesiniak, M.; Fenniri, H.; Webster, T.; Rao, R.D.; Zhang, L.G. 3D Printed scaffolds with hierarchical biomimetic structure for osteochondral regeneration. *Nanomedicine* **2019**, *19*, 58–70. [CrossRef] [PubMed]